Bioprinting 14 (2019) e00045

Contents lists available at ScienceDirect

Bioprinting

journal homepage: www.elsevier.com/locate/bprint

Bio-fabrication of peptide-modified alginate scaffolds: Printability, mechanical stability and neurite outgrowth assessments

M.D. Sarker [a,*], Saman Naghieh [a], Adam D. McInnes [a], Liqun Ning [b], David J. Schreyer [c], Xiongbiao Chen [a,b]

[a] Division of Biomedical Engineering, College of Engineering, University of Saskatchewan, Saskatoon, SK, Canada
[b] Department of Mechanical Engineering, College of Engineering, University of Saskatchewan, Saskatoon, SK, Canada
[c] Department of Anatomy and Cell Biology, College of Medicine, University of Saskatchewan, Saskatoon, SK, Canada

ARTICLE INFO

Keywords:
Alginate
Peptide
3D bio-printing
Printability
Nerve regeneration
Tissue engineering
Scaffold

ABSTRACT

Peripheral nerve tissue requires appropriate biochemical and physical cues to guide the regeneration process after injury. Bioprinted peptide-conjugated sodium alginate (PCSA) scaffolds have the potential to provide physical and biochemical cues simultaneously. Such scaffolds need characterisation in terms of printability, mechanical stability, and biological performance to refine and improve application in nerve tissue regeneration. In this study, it was hypothesized that 3D scaffold printed with low concentrated multiple PCSA precursor would be supportive for axon outgrowth. Therefore, a 2% (w/v) alginate precursor was conjugated with either arginine-glycine-aspartate (RGD) or tyrosine-isoleucine-glycine-serine-arginine (YIGSR) peptides, or a mixture of RGD and YIGSR (1:2) and was bioprinted in this study. The printability of the composite PCSA scaffolds was tested in three different concentrations of crosslinker (i.e. 50, 100, and 150 mM of $CaCl_2$), and was evaluated by measuring strand width, pore geometry, and angle-formation accuracy. Swelling, degradation, and compression experiments were conducted over a 3 week period to evaluate the mechanical stability of the composite PCSA scaffolds. Scanning electron microscopic (SEM) images were taken to study the surface morphology of the degraded scaffolds. Biological performance was assessed both for single and composite PCSA scaffolds by quantifying the viability and morphology of seeded or incorporated Schwann cells (SCs), amount of secreted brain derived neurotrophic factor (BDNF) by incorporated SCs, and directional neurite outgrowth of neuron cells in a 2D culture. Experimental results suggest that 30 kPa extrusion pressure and 18 mm/s needle speed are suitable to fabricate composite PCSA scaffolds with reasonable strand or pore printability (~0.95–1.0), and 50 mM $CaCl_2$ facilitated better strand and pore printability than the two other concentrations. Captured SEM images demonstrate that all the composite PCSA scaffolds preserved the initial biofabricated porous structure over 3 weeks, but they lost ~70% of the initial elastic modulus. In terms of biological performance, composite PCSA scaffolds facilitated better viability and morphology of SCs, as well as supported superior directional neurite outgrowth compared to that of a single PCSA scaffold.

1. Introduction

Peripheral nervous system (PNS) injuries lead to painful neuropathies, poor sensational responses, as well as reduced function in muscles and organs. Significant progress in tissue engineering [1–5], research over the past decades has opened up the vast possibility to regenerate nerve tissue across a critical gap (>2 mm) with biofabricated scaffolds [1,6–8]. In biofabrication, hydrogels, particularly sodium alginate (SA), has frequently been studied and considered as a suitable biopolymer for biocompatibility due in part to being hydrophilic [2,9–12]. However, SA lacks cell binding motifs in its molecular structure and has poor mechanical strength [13].

A number of studies investigated the printability of SA or SA composites, as well as the mechanical property (i.e. swelling, degradation, elastic modulus, etc.) of SA scaffolds incubated in DMEM or physiologic buffer over specific time points [14–16]. Several studies have used single PCSA (i.e. RGD, YIGSR, etc.) hydrogels to investigate its biological performance in tissue regeneration [17–19]. However, studies focusing on

* Corresponding author.
E-mail address: mas921@mail.usask.ca (M.D. Sarker).

https://doi.org/10.1016/j.bprint.2019.e00045
Received 22 November 2018; Received in revised form 27 January 2019; Accepted 31 January 2019
2405-8866/© 2019 Elsevier B.V. All rights reserved.

the printability of composite PCSA precursors in ionic crosslinkers and the mechanical stability of composite PCSA scaffolds remains unexplored thus far. Preparation of composite PCSA is a multistage chemical process, and there is a possibility that the chemical treatment might alter the molecular structure, orientation, and physical properties of SA. Since these properties affect the mechanical stability, viscosity, and printability of hydrogels, a systematic study is required to characterize the composite PCSA precursor for their possible application in nerve tissue regeneration.

Since SCs play a significant role in axon regeneration by upregulating numerous biochemical signals and forming 'band of Büngner', the effect of single or composite PCSA scaffolds on the biological activity of SCs needs to be evaluated. Although some studies have investigated the effect of a single PCSA hydrogel on the biological function of SCs [20], the comparative studies between a single and composite PCSA scaffolds affecting the biological activities (e.g. 3D viability, morphology, cell processes length, and growth factor secretion) of SCs remains unstudied till now. But this type of study is required to understand the effectiveness of the conjugation of multiple peptides on the molecular chain of SA for nerve tissue regeneration.

Stimulated neuron cells are more representative of *in vivo* dorsal root ganglion neurons after nerve injury compared to unstimulated neuron cells. Two-dimensional culture of stimulated neurons on PCSA strands closely simulate the *in vivo* neurite outgrowth through the developing growth cone. Although a number of studies have investigated neurite growth on a patterned substrate [21,22], the study of stimulated neuron cell culture on a single or composite PCSA strands remains unexplored. Since nerve regeneration requires directional outgrowth of neurites, the effect of PCSA pattern on the directional growth of neurites needs to be assessed.

In this study, the printability of composite peptide (i.e. RGD and YIGSR) conjugated 2% SA precursor in three different concentrations of $CaCl_2$, 50, 100, and 150 mM, were evaluated by comparing the bioprinted strand width, pore shape, and angular structure with theoretical or computer-aided design (CAD) data. Mechanical stability, particularly swelling, degradation, and elastic modulus were measured by incubating the composite PCSA scaffolds in physiologic buffer (10 mM PBS) over 3 weeks. To investigate morphological changes, the degraded scaffolds were assessed by capturing SEM images. The 2D morphology of primary rat SCs (RPSCs) on RGD, YIGSR, and composite peptide-conjugated 2% SA hydrogel was studied over a 3-day culture period. The viability and morphology of RPSCs incorporated into PCSA strands were studied over a 7-day culture period. The amount of released BDNF by incorporated RPSCs in the PCSA strands over a 3-day culture period was measured using ELISA kits. To harvest stimulated neuron cells, the sciatic nerve was transected two days prior to sacrifice, and the harvested neuron cells were cultured for 7 days on the PCSA strands to assess the directional neurite outgrowth.

2. Materials and methods

2.1. Materials

Medium-viscosity sodium alginate, MES buffer, N-hydroxysuccinimide (NHS), N-(3-dimethylaminopropyl)-N′-ethylcarbodiimide hydrochloride (EDC), calcium chloride ($CaCl_2$), polyethyleneimine (PEI), Tween 20, Hoechst 33342, mouse β-III tubulin and bovine serum albumin (BSA) were purchased from Sigma-Aldrich, ON, Canada. The GIBCO Life Technologies (Burlington, ON, Canada) was the supplier of calcium-free and standard DMEM media. For the immuno cytochemistry experiment, rabbit anti-S100 was purchased from Abcam (Eugene, OR, USA), whereas AF 488 anti-mouse IgG, 4′, 6-diamidino-2-phenylindole (DAPI), and AF 555 anti-rabbit IgG antibodies were procured from Thermo Fisher Scientific, MA, USA. In addition, calcein-AM (1 μg/ml), propidium iodide (10 μg/ml), RGD (GGGGRGDS), and YIGSR peptides were purchased from Anaspec (Freemont, CA, USA).

2.2. Alginate modification

In this study, single (YIGSR or RGD) and dual peptides were linked to sodium alginate molecule using covalent chemistry reported elsewhere [23]. For single peptide conjugate reactions, 1 mg RGD or YIGSR was added to per gram alginate, while for composite peptide conjugate reactions RGD and YIGSR was added to alginate maintaining 1:2 M ratio. The RGD peptide was reported to affect the adhesion and proliferation of PC12 cells, while the YIGSR peptide was found to regulate neuronal differentiation at an elevated density [24]. Therefore, in this study RGD and YIGSR peptide sequences have been covalently linked with alginate hydrogel maintaining a 1:2 M ratio to enhance the adhesion of neuron cells and axon outgrowth. Initially, an alginate solution (1% w/v) was sterilized using 0.2 μm filter (Thermo Scientific Nalgene), and freeze-dried for 48 h. The freeze-dried alginate was dissolved in water containing 0.1 M MES buffer and 0.3 M NaCl. The pH of the solution was maintained at 6.5 for optimal reaction kinetics for binding peptides to alginate molecules. Sulfo-NHS, a stabilizer for covalent reactions, was added in the solution, maintaining a ratio of 1:2 to EDC. A magnetic stirrer was used to mix the sulfo-NHS with the alginate solution for 20 min. EDC was added next to activate 40% of the available uronic acid residues on the alginate molecules in the solution (300 mg EDC/g alginate), and stirred for 10 min. After sufficient mixing, the peptides were added to the solution, and the covalent reaction was allowed to proceed for 48 h at 20 °C under mild stirring. To purify the reaction mixture by-products, salt, buffer, and any unwanted molecules, the experimental solution was dialyzed with Spectra/Por dialysis tubing (MWCO 12-14000). Since precipitation technique using chemicals might affect the PCSA precursors, the dialysis method has been used in this study to get rid of tiny unwanted molecules. In the dialysis process, 40 L of deionized water was used to increase the purity of peptide-alginate conjugate over a period of 5 days. The final step was to freeze dry the dialyzed solution, and resolubilize the modified alginate as required.

2.3. Preparation of rat primary Schwann cells (RPSCs)

To harvest RPSCs, the sciatic nerve was isolated from Sprague-Dawley rats, the epineurium was dissected off, and the denuded nerve was cut into small segments. All the surgical procedures of rodents were conducted as per the approval of the University Committee on Animal Care and Supply (University of Saskatchewan). The segments were digested in collagenase (1 μg/ml) at 37 °C for 1 h, then the digested solution was filtered to remove the ECM debris. To stimulate Schwann cell proliferation and inhibit fibroblast growth, the filtered cells were cultured in Dulbecco's Modified Eagle Medium (Saint Louis, MO, USA) containing D-valine, 10% fetal bovine serum, forskolin, and bovine pituitary extract added N-2 supplement [25]. Immunofluorescence assays with S-100 and DAPI were used to evaluate the purity of the collected cells (i.e. RPSC) in culture. The cultures were incubated in a tissue culture dish (Thermo Fisher Scientific, Rochester, NY, USA) at 37 °C in a 5% CO_2-enriched humidified incubator to achieve 100% confluency.

After reaching 100% confluency, RPSCs were detached from the tissue culture plate using 1 ml 0.25% Trypsin/EDTA (Invitrogen) and suspended in 10 ml DMEM supplemented with 10% fetal bovine serum. To prepare sufficient density, the cell suspensions were transferred to 50 ml centrifuge tubes (Falcon®, Mexico) and centrifuged for 5 min at 108 g while maintaining 4 °C. The cell pellet was resuspended in 250 μl DMEM, and the cell concentration was determined using a haemocytometer. The cell density was adjusted by adding an appropriate amount of DMEM to achieve the desired density for 2D and 3D culture. For 2D and 3D RPSC culture, cell density was maintained as 2.5×10^4 cells/cm^2 and 2×10^5 cells/ml hydrogel, respectively.

2.4. Bio-fabrication of scaffold

A pneumatic 3D Bioplotter (EnvisionTEC, Germany) was used in this

study to print 2D pattern as per a predefined design. CAD software was used to develop a cuboid shape (10 mm × 10 mm x 5 mm) with 1 mm interstrand distance. To study Schwann cell viability in the bio-printed strand, double-layered grid patterns were fabricated by alternating perpendicular layers. The pattern was printed on a 12-well tissue culture using a 200 μm tapered needle. The needle speed and dispensing pressure were maintained as 18 mm/s and 0.3 bar, respectively, in printing alginate (2% w/v) strands. Calcium-free DMEM solution was used to prepare a 2% (w/v) solution of pure alginate or peptide conjugate alginate. To prepare alginate/cell mixture, RPSCs were trypsinized upon 100% confluency, and then thoroughly mixed with alginate (2% w/v) solution keeping cell density as 2×10^5 cells/ml. To study neurite extension from neuron cells, single layered patterns were bioprinted in each well of a 12 well tissue culture plate.

Alginate doesn't attach to bare tissue culture plates. To enhance the adhesion property, 1 ml PEI (0.1% w/v) was added in each well of a 12 well plate and incubated overnight at 37 °C with 5% CO_2. Before printing, the PEI solution was aspirated from the well, and three successive wash was conducted with 10 mM PBS. Then, 1 ml $CaCl_2$ (50 mM) solution was dispensed in each well to serve as a crosslinker. The 2D pattern was printed into the $CaCl_2$ solution where the Ca^{2+} rapidly crosslink the hydrogel precursor. The printed cell/alginate mixture was kept in the crosslinker solution for 2 min to promote uniform crosslinking. Following crosslinking, the $CaCl_2$ solution was aspirated from the well, and the pattern was washed with 10 mM PBS. One milliliter of cell culture media (90% DMEM + 10% FBS) was added to each well of the tissue culture plate, which was then placed in an incubator.

2.5. Assessment of printability

To evaluate 2D and 3D printability, peptide-modified alginate scaffolds were printed maintaining various extrusion pressure (i.e. 20, 30, and 40 kPa) and linear needle speed (i.e. 6, 8, 10, 12, 14, 16, 18, 20, 22, 24, and 26 mm/s). The concentration of hydrogel precursor was kept as 2% (w/v), while the concentration of $CaCl_2$ solution was varied between 50 and 150 mM. Printability of composite PCSA strands was evaluated in terms of strand diameter, interstrand distance, pore geometry, and interstrand angle (Fig. 1). These parameters were compared with expected or CAD-generated geometry. The expected strand diameter as per [26]:

$$D_s = \sqrt{\frac{4Q_t}{\pi V_n}} \tag{1}$$

where D_s, V_n, and Q_t represent strand diameter, linear needle speed, and volumetric flow rate of hydrogel precursor, respectively. Similarly, printability of a square pore was calculated as per [27]:

$$P_r = \frac{P^2}{16A} \tag{2}$$

where P_r, P, and A represent the pore printability, perimeter of a pore, and area enclosed inside a pore, respectively. To measure the printability of alginate strands in an angular fashion, strands were printed at interstrand angles of 27°, 45°, and 60° that were assigned in the CAD program. The printability of strand width, interstrand gap, and angular geometry were measured as follows:

$$P_D = \frac{D_T - D_E}{D_T} \text{ x } 100\% \tag{3}$$

where P_D, D_T, and D_E represent dimension printability, theoretical dimension, and experimentally obtained dimension, respectively. A fluorescent microscope (Carl Zeiss Axiovert 100) was used to capture the images of printed strands from a random spot and the best representative images were selected for demonstration and calculation purpose. All the dimensions were precisely measured using ImageJ software (National Institutes of Health, Bethesda, Maryland, U.S.A.) and at least three replicates were maintained for each experiment for statistical significance.

2.6. Swelling, degradation and compression test

To assess the swelling characteristics of composite PCSA scaffold, 10 mM phosphate buffered saline (PBS) was used in this study. PBS buffer was used to evaluate the influence of Na^+ ions on the degradation of

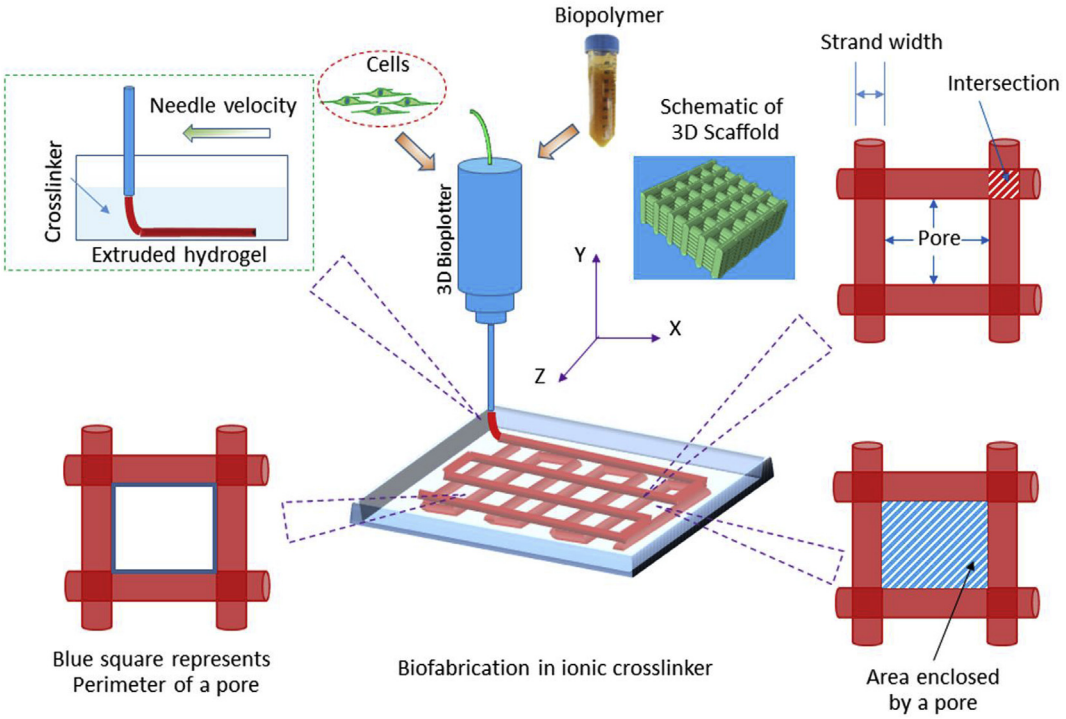

Fig. 1. Schematic of a printed pattern in an ionic crosslinker indicating strand diameter, perimeter of a pore, and area enclosed inside a pore.

composite PCSA scaffolds. However, in the future study, simulated body fluid (SBF) is recommended to evaluate the effect of multiple ions on the degradation of PCSA scaffolds. Briefly, after 3D printing, the scaffolds were immersed in 2 ml PBS and incubated in CO_2 at 37 °C for predetermined time intervals. In particular, swelling was measured at 1, 2, 3, 24, 48, 168, and 336 h after removing the free buffer from the scaffold pores by blotting with Kimwipes™ using the formula;

$$SI = \frac{M_t - M_0}{M_0} \text{x } 100 \quad (4)$$

where SI, M_t, and M_0 represent swelling index, wet weight of scaffolds at time intervals (t), and initial wet weight of scaffolds, respectively. To obtain the initial weight, the scaffolds were taken out from crosslinker immediately after fabrication, blotted with Kimwipes™, and weighed on a scale. For each time point, swelling data was collected for three replicates.

Scaffold degradation was measured by incubating them in 10 mM PBS solution for particular time points. All the scaffolds were freeze-dried for 2 days and then weighed to obtain initial mass. The freeze-dried scaffolds were immersed into 2 ml PBS and incubated at 37 °C in 5% CO_2 for 3, 7, 14, and 21 days. At the scheduled time point, the scaffolds were collected, further freeze dried and weighted to obtain the final weights. The scaffold degradation in terms of percentage mass loss was calculated using:

$$M_L = \frac{M_0 - M_t}{M_0} \text{x } 100 \quad (5)$$

where M_L, M_0, and M_t represent percentage (%w/w) mass loss, initial freeze-dried mass and freeze-dried mass at specific time points (t), respectively. To evaluate statistical significance, degradation data was collected for three replicates.

To assess the elastic modulus of 3D printed scaffolds incubated in physiological buffer (i.e. PBS) for a different time period, compressive force was applied to the scaffolds using a texture analyzer machine (Texture Technologies, MA, U.S.A.). Briefly, after 3D fabrication, the scaffolds were immersed into 2 ml PBS and incubated at 37 °C in 5% CO_2 for a period of 7, 14, and 21 days. The scaffolds were taken out of the 12-well tissue culture plate at scheduled time intervals, excess buffer solution was blotted with Kimwipes™, and the scaffolds positioned between the probes of texture analyzer machine to measure the elastic modulus. The scaffolds were compressed up to 20% of their original thickness while maintaining a uniform probe speed of 0.01 mm/s. For each time interval, compression testing was conducted on three replicates to evaluate the statistical significance. The data obtained from texture analyzer machine was compressive force versus deformation, and dividing them by area and height result in applied stress versus strain. To obtain the area and height, the images of the associated scaffolds were captured, and processed with ImageJ software. The slope of stress versus strain curve up to yield point was considered as Young's modulus.

2.7. Scanning electron microscopy (SEM)

To assess the surface morphology of scaffolds at different time points (i.e. day 0, 14, and 21), scanning electron microscopic images were captured using a SEM machine (Hitachi SU8000, Japan). Briefly, the scaffolds were collected at different time intervals and freeze-dried for 2 days, then positioned on carbon tape attached SEM stubs, and coated with 10 nm gold layer (Q150T, Quorum Technologies, U.K.). Microscopic images were captured from arbitrary sites on the scaffolds at 5 kV machine voltage and the most representative images of the surface morphology are shown in this study for qualitative analysis.

2.8. Preparation of 2D surface and RPSC culture

The 2D alginate surface was prepared on round glass coverslips. To prepare the coverslips, 1 ml PEI (0.1% w/v) was used to coat the 2D surface overnight at 37 °C in an incubator. The PEI was aspirated, and slides were washed with 10 mM PBS buffer. 100 µl (2% w/v) of RGD, YIGSR, and RGD/YIGSR-conjugated 2% alginate, and 2% pure alginate precursor were dispensed on the cover glass. The hydrogel precursor was crosslinked with 50 mM $CaCl_2$ for 1 h to obtain a flat 2D surface. To prepare a positive control, 1 ml PLL solution was dispensed into each well of a 12-well plate and kept in an incubator (37 °C) overnight to ensure coating. Prior to cell culture, PLL was aspirated from the well, and 10 mM PBS buffer was used to wash the well properly. RPSCs were seeded on the top of 2D surface and cultured for 3 days at 37 °C in a 5% CO_2 enriched humidified incubator.

2.9. Cell viability study

The viability of Schwann cells incorporated in the bioplotted strand was assessed using a live and dead cell staining assay at day 0, 3, and 7. Since the harvested neuron cells were cultured for 7 days period in this study, the viability and morphology of RPSCs were also investigated for 7 days to maintain the consistency with the neuron cell culture. On the scheduled period, culture media (90% DMEM+10% FBS) was aspirated from 12-well plate, and the culture plate was washed two times with 10 mM PBS. Then, 1 ml fresh culture media containing 2 µl of propidium iodide (5 µg/ml) and calcein-AM (1 µg/ml) were added in each well of the culture dish. The culture was incubated for 2 h at 37 °C with 5% CO_2. Prior to imaging, culture media was aspirated, and each well was washed thoroughly with 10 mM PBS three times to get rid of the free staining agent. Using a fluorescent microscope (Axiovert 100, Zeiss), multiple images were taken at different depths at selected spots in the bioplotted strands. The best representative spot of the 3D culture in the strands was chosen to evaluate the cell viability. ImageJ (National Institutes of Health, MD, USA) software was used in stacking the multiple images and measuring total dead and live cell population. The cell viability was calculated using the equation:

$$V\,(\%) = \frac{C_L}{C_L + C_D} \text{x } 100 \quad (6)$$

where C_L, C_D, *and* V represent the live cells, dead cells, and cell viability, respectively.

2.10. BDNF-release assessment

Assaying of the release of brain-derived neurotrophic factor (BDNF) conducted in this study with ELISA kit (BDNF Emax® ImmunoAssay Systems - Promega Corporation, USA). A 96-well ELISA plate was coated with anti-BDNF mAb in carbonate buffer overnight at 4 °C. The coating solution was flicked out, and the wells were washed with TBST wash buffer. To block the nonspecific binding sites on the well, blocking buffer was added in each well and incubated 1 h at room temperature. Following well blocking, the blocking solution was flicked out properly and TBST buffer was used to wash the wells. To prepare a standard curve, two rows of wells were used. Diluted BDNF standard (500 pg/ml) was added to the first well of each row and 1:2 serial dilutions were conducted down to the last well of each row. To prepare test samples, printed strands of Schwann cells (2×10^5 cells/ml) incorporated into various alginate-peptide combination hydrogels were cultured for 3 days. For a particular sample, the scaffold was fabricated dispensing 100 µl PRSC/biopolymer mixture using a 3D bioplotter. At least 3 scaffolds were printed in a 12-well tissue culture plate for a specific sample. For positive control (i.e. PLL-coated plate), 2×10^4 PRSCs were seeded and conducted 2D culture for 3 days. Since BDNF demonstrates a short half-life, a long period of RPSCs culture might not significantly enhance the amount of released BDNF in the hydrogel. Accordingly, in this study a 3 days culture period of RPSCs was chosen instead of 7 days [28]. From each culture, 100 µl of supernatant was collected and added in the nonspecific sites

blocked wells of ELISA plate. BDNF-standard- and test-sample-loaded wells were incubated in a shaker at room temperature for 2 h. After 5 successive washes, diluted Anti-Human BDNF pAb in block buffer was added in each well and the ELISA plate was incubated in a shaker at room temperature for 2 h. The wells were vacated through flicking out the added solution followed by 5 consecutive washes. Then diluted Anti-IgY HRP in block buffer was added in each well and the ELISA plate was incubated in a shaker at room temperature for 1 h. Finally, after flicking out the solution and sequential washing of the wells, 100 µl TMB one solution was added to each well. The ELISA plate was incubated at room temperature in a shaker for 10 min, then the reaction was terminated by adding 100 µl 1 N hydrochloric acid to each well. The absorbance of yellow color by the solution in each well was measured with a plate reader at 450 nm wavelength.

2.11. Dorsal root ganglion (DRG) harvest, culture, and immunocytochemistry

To stimulate the growth of the DRG neurons, the left sciatic nerves of the rats were lesioned two days prior to sacrifice (Fig. 2). Fifteen male Sprague-Dawley rats (weight 250–300 g) were randomly distributed into 3 groups (n = 5), and all received the following procedure. To prepare for the surgical procedure, 1.5–2% isoflurane was used to anesthetize the rats, and the flow rate of isoflurane and oxygen was maintained as 0.8–1 L/min. During the procedure, a skin incision was made along the femoral axis, then blunt dissection of the underlying muscles was conducted to reach the sciatic nerve, and then the nerve was transected. At the end of the procedure, 4-0 silk was used to close the incision in the skin. All the surgical procedures were conducted under sterile conditions. The animals were given analgesic buprenorphine injections (0.05 mg/kg) every 8 h for 2 days postoperatively. Two days after the surgery, all the animals in the groups were sacrificed.

The dorsal root ganglia of the sciatic nerve plexus (L4-L6) were excised from the rats, collected in L15 media, and spun at 108 g for 5 min to collect the DRG pellets. To dissociate the neurons in the DRGs, the pellets were incubated with collagenase (1 µg/ml) for 1 h at 37 °C, triturated using a series of serum-coated Pasteur pipettes having large to narrow openings, and further treated with trypsin (0.75 µg/ml) for an extra 30 min. Then cold horse serum was added to quench trypsin activity, a 100 µm cell strainer was used to filter the ECM debris, and 15% bovine serum was added to form a layered cell suspension. After spinning the suspension at 121 g for 20 min, the supernatant was aspirated to isolate the neuron cell pellet, and DMEM was added to resuspend the neuron cell population. Finally, 1000 neuron cells were seeded on each single-layered alginate-peptide scaffold incorporated with SCs and cultured for 7 days in DMEM with 10% horse serum. PLL-coated wells seeded with neuron cells at the same density were used as a positive control. In particular, the co-culture of neuron cells and RPSCs was conducted incorporating RPSCs inside the 3D bioprinted strands and seeding neuron cells on the top of the strands.

To conduct immunocytochemistry, after 7 days, the media was aspirated from tissue culture well, and the cultures were thrice thoroughly washed with 10 mM TBS. Cold methanol (−20 °C) was used to fix the cultures for 2 h. After fixation, methanol was aspirated and the cultures were rinsed properly with TBS. Then the cultures were treated with blocking solution (10 mM TBS, 0.5% bovine serum albumin, 2% horse serum, 0.05% Tween 20) for 2 h at room temperature to prevent background staining. Primary antibody rabbit anti-S-100 and mouse anti-βIII tubulin (1:1000; Sigma Aldrich) was added to the blocking solution to bind with specific proteins expressed by Schwann cells and axons, respectively, and incubated for 2 h at room temperature. To remove any remaining free antibodies, the cultures were thoroughly rinsed five times by immersing the scaffolds in TBS for 10 min each time. Blocking solution containing two secondary antibodies and DAPI (1 µM) was added next and incubated for 2 h at room temperature to fluorescently stain the Schwann cells, axons, and nuclei, respectively; specifically, Alexa Fluor 488 goat anti-mouse and Alexa Fluor 555 goat anti-rabbit immunoglobulin (1:500; Thermo Fisher Scientific) were used as secondary antibodies. Then the samples were washed thoroughly five times with TBS and mounted on glass slides using ProLong Gold antifade mountant (Thermo Fisher Scientific). Confocal laser scanning microscopy (Leica SP5, Germany) was used to capture 2D images layer-by-layer. OrientationJ and NeuronJ were used to assess the orientation and length of neurites on the patterned scaffold.

To study Schwann cell processes in a 3D scaffold, a similar protocol was followed to conduct the immunocytochemistry, where mouse anti-S-100 and Alexa Fluor 488 goat anti-mouse were used as primary and secondary antibody, respectively. A fluorescence microscope (Axio Imager M1, Zeiss) was used to capture 2D images. For a particular location, 2D images were captured successively at a different height.

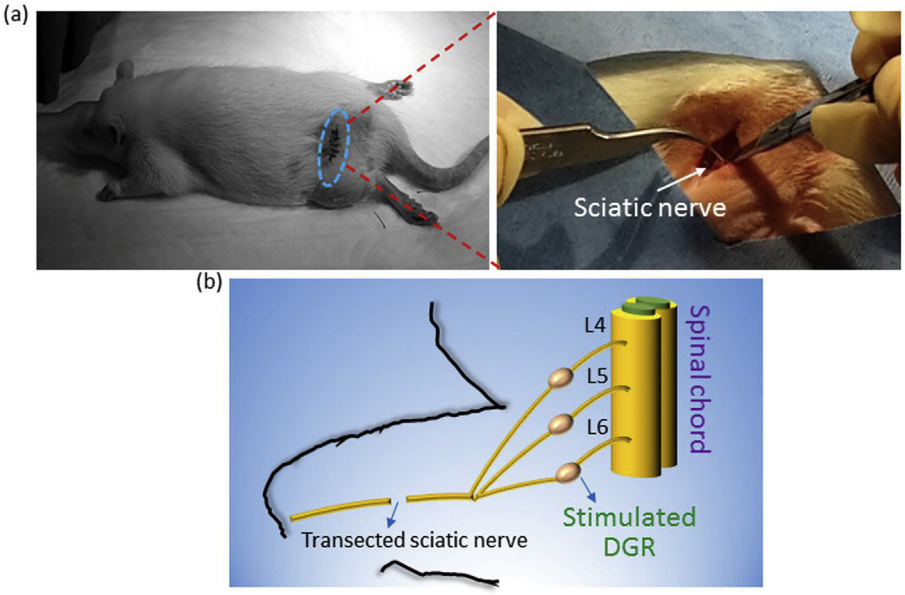

Fig. 2. Sciatic nerve transection to stimulate DRG neurons; (a) sciatic nerve transection of a Sprague-Dawley rat, (b) schematic of transected sciatic nerve and associated DRGs.

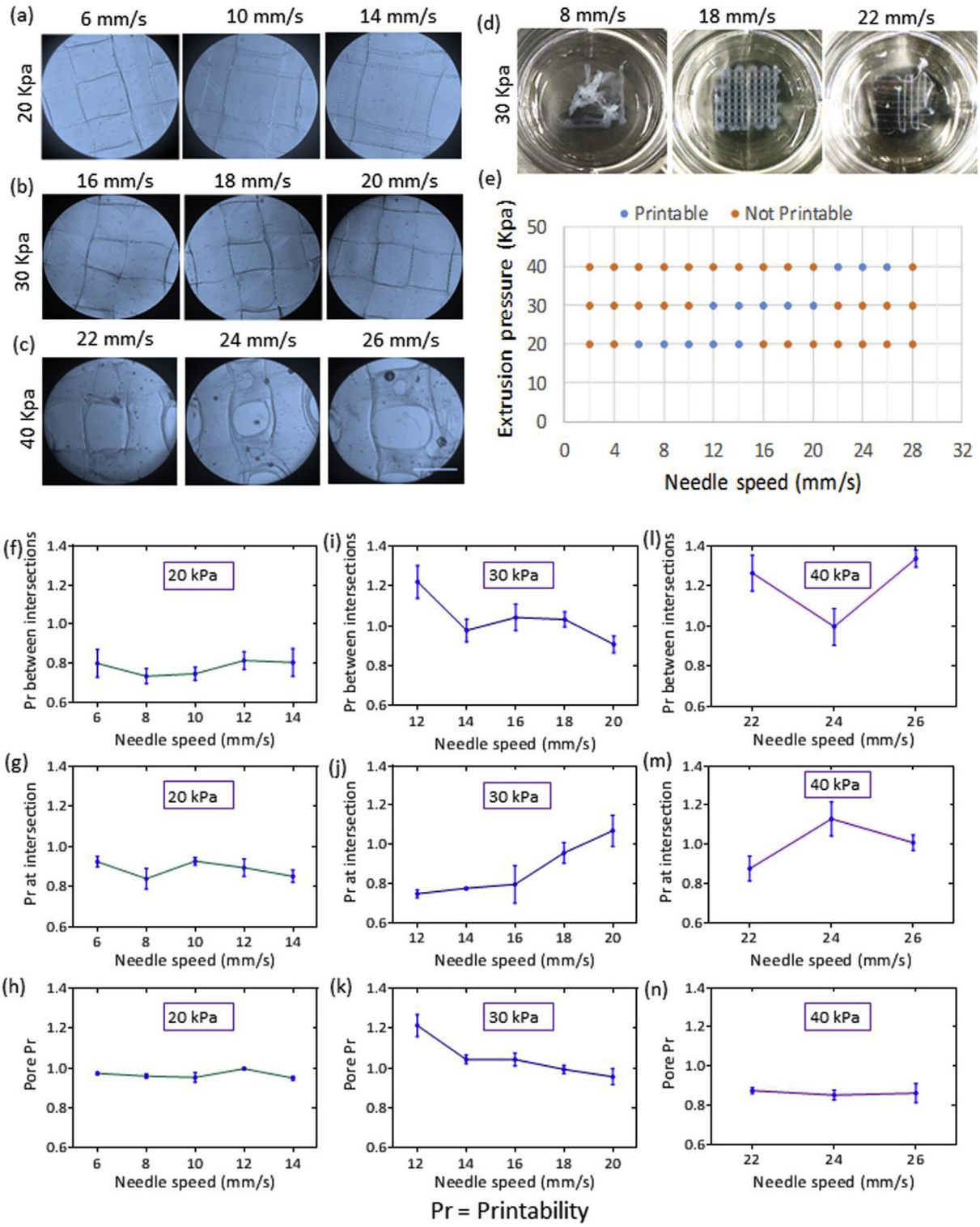

Fig. 3. Two-dimensional printability of RGD/YIGSR-alginate conjugate precursor: (a–c) microscopic images of alginate strands bioprinted using various pressures, (d) printable and non-printable structures at 30 kPa extrusion pressure and different needle speeds, (e) plot representing the range of printable and non-printable pressures at the elevated needle speeds, (f, i, and l) strand printability between intersections at extrusion pressures 20, 30, and 40 kPa with respect to various needle translation speeds, (g, j, and m) strand printability at intersections at extrusion pressures 20, 30, and 40 kPa with respect to various needle translation speeds, and (h, k, and n) pore printability at extrusion pressures 20, 30, and 40 kPa with respect to various needle translation speeds.

Three-dimensional images were built by stacking multiple 2D images with ImageJ software. For each experiment, images were captured from random locations, and the best representative images were shown in this study.

2.12. Statistical significance

To measure statistical significance between two sets of data, Student's t-test was conducted with Graph Pad Prism 5.0a software (GraphPad Software, San Diego, CA, USA). A cut-off of $p < 0.05$ was used to

determine statistical significance. Experimental results were presented as the mean and standard deviation (SD) of the calculated data.

3. Results

3.1. Printability of double layered pattern

Experimental results suggest that extrusion pressure and needle translation speed regulate the strand width and printability of hydrogel precursors in ionic crosslinkers. For a particular extrusion pressure, the strand width decreases with the increase of needle translation speed (Fig. 3(a–c)). At a particular extrusion pressure, biofabrication seems to be possible for a range of linear needle translation speed. Below or above the limit, excess accumulation or inadequate build-up of biopolymer on the printing surface result in fabrication complexities (Fig. 3(d and e)).

The effect of extrusion pressure and needle translation speed on strands printability in terms of the overall structure and strand width have been presented in Fig. 3(f-n). In this study, printed strands demonstrated nonuniformity in width along the direction of fabrication. Two-dimensional scaffold printability was measured by comparing strand width at the intersections, strand width between intersections, as well as the pore shape to the theoretical values. As the dimensions of bioprinted scaffolds approach the theoretical value, the printability value becomes 1. Since the experimental value always differs from the theoretical one, in this study the acceptable value of printability has been considered as 1 ± 0.1.

In this study, keeping the concentration of $CaCl_2$ constant (i.e. 50 mM), three different extrusion pressures (i.e. 20, 30, and 40 kPa) were applied to print 3D patterns of 2% (w/v) composite PCSA precursor using a 200 μm needle. A minimum dispensing pressure of 20 kPa was chosen to avoid fabrication problems in the 3D scaffolds. At an extrusion pressure of 20 kPa, the strand printability at the intersection was measured as ~ (0.90–0.95) for needle translation speeds of 6 and 10 mm/s, while ~ (0.8–0.9) printability was noticed for 8, 12, and 14 mm/s needle translation speeds (Table 1). However, the strand printability between the intersections was inferior ~ (0.7–0.85) for all speeds compared to those at the intersections. In contrast, the pore shape printability was superior ~ (0.95–1) to both the strand width measured at the intersections and between intersections. At this pressure, scaffold fabrication seemed possible for needle translation speeds between 6 and 14 mm/s.

At an elevated extrusion pressure (i.e. 30 kPa), reasonable strand printability ~ (0.9–1.1) was identified at the intersections and between intersections for 18 and 20 mm/s needle translation speeds, respectively, with 18 mm/s seeming to be ideal for all values. The scaffold pores were close to a perfect square and showed a reasonable printability value ~ (0.95–1.05) for 14–18 mm/s needle translation speed. However, 30 kPa pressure allowed biofabrication only for 12–20 mm/s linear needle translation speed. Further increasing the extrusion pressure to 40 kPa constricted the range of needle translation speed to 22–26 mm/s, for which 3D scaffold fabrication is possible. At this pressure, strand printability at the intersections and between intersections was calculated as ~ (0.8–1.2) and (0.9–1.35), respectively. In particular, strand printability becomes unpredictable at elevated needle translation speeds. The pores generated at these faster speeds demonstrated unsatisfactory printability (~0.8–0.9).

Strand and pore printability at different extrusion pressures and needle translation speeds that fall in the range of reasonable printability (0.9–1.1) have been highlighted in the results listed in Table 1. For extrusion at 20 kPa, the strand width and pore shape were found to be under printed (i.e. <1) at all needle translation speeds calculated using formula (1). In contrast, at pressures of 30 and 40 kPa, the strand widths and pore shape were found either under or over printed (i.e. <1 or >1) at different needle translation speeds (Table 1). These results suggest that both needle translation speed and extrusion pressure affect the dimension of bioprinted strands. However, 40 kPa resulted in non-uniform strands that led to poor printability (Fig. 3(l–n)). Table 1 suggests that only extrusion pressure at 30 kPa and needle translation speed of 18 mm/s ensure outstanding strand and pore shape printability. Therefore, the pressure and needle translation speed are recommended to fabricate the composite PCSA scaffolds with 200 μm needle in the 50 mM $CaCl_2$ solution.

3.2. Printability of angular pattern

Biofabrication of complex structure or organ often requires extrusion of the hydrogel precursor in an angular fashion [14]. Therefore, in this study, angle printability of composite PCSA precursor was evaluated with respect to CAD data using formula (3). Since extrusion pressure at 30 kPa and needle translation speed at 18 mm/s resulted in superior strand printability, strands were printed using this pressure and speed in the 50 mM $CaCl_2$ solution. Under these conditions, no overlap or accumulation was noticed at the intersections (Fig. 4(a–d)). The angle printability was measured as 1.073 ± 0.12, 1.03 ± 0.03, 1.047 ± 0.06, and 1 ± 0.02 for 27°, 45°, 60°, and 90° angles that were assigned in the CAD parameters, respectively. Compared to strands at right angles, strands extruded at acute angles showed more deviation from the CAD parameters (Fig. 4(e)). However, all the angles printed with the alginate

Table 1
Strand width printability with various extrusion pressures and needle translation speeds (highlighted data in red represents reasonable printability ranging from 0.9 to 1.1).

Extrusion Pressure (Kpa)	Printability	Needle Speed (mm/s)				
		6	**8**	**10**	**12**	**14**
20	At intersections	0.925 ± 0.025	0.84 ± 0.052	0.928 ± 0.019	0.895 ± 0.044	0.853 ± 0.03
	Between intersections	0.8 ± 0.07	0.735 ± .039	0.748 ± 0.033	0.815 ± 0.045	0.805 ± 0.07
	Pore structure	0.973 ± 0.006	0.96 ± 0.01	0.953 ± 0.025	0.997 ± 0.006	0.95 ± 0.01
		12	**14**	**16**	**18**	**20**
30	At intersections	0.75 ± 0.02	0.778 ± 0.005	0.798 ± 0.095	0.958 ± 0.052	1.07 ± 0.079
	Between intersections	1.22 ± 0.082	0.978 ± 0.056	1.043 ± 0.067	1.033 ± 0.038	0.908 ± 0.042
	Pore structure	1.213 ± 0.06	1.043 ± 0.02	1.043 ± 0.03	0.993 ± 0.02	0.957 ± 0.04
		22		**24**		**26**
40	At intersections	0.878 ± 0.063		1.13 ± 0.086		1.01 ± 0.039
	Between intersections	1.265 ± 0.09		0.998 ± 0.092		1.338 ± 0.043
	Pore structure	0.877 ± 0.015		0.853 ± 0.025		0.863 ± 0.049

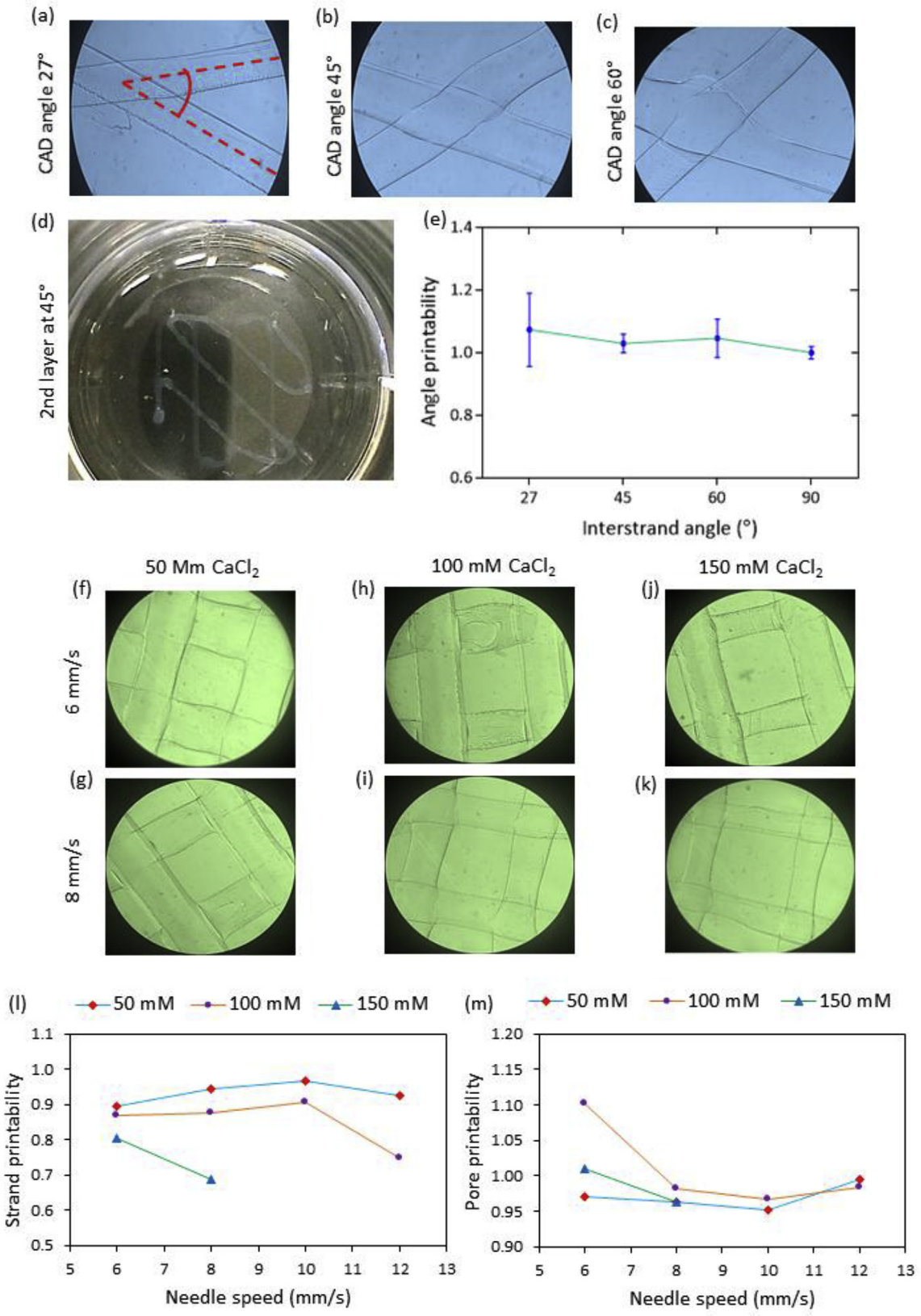

Fig. 4. Printability of RGD/YIGSR-alginate conjugate strands with respect to angular geometry and varying concentration of $CaCl_2$; CAD angle (a) 27°, (b) 45°, and (c) 60°; (d) macroscopic image of extruded strands bioprinted at 45° CAD angle; (e) plot of angel printability with respect to CAD angle; macroscopic images of composite PCSA strands extruded into 50 mM $CaCl_2$ at (f) 6 mm/s and (g) 8 mm/s needle speed, 100 mM $CaCl_2$ at (h) 6 mm/s and (i) 8 mm/s needle speed, and 150 mM $CaCl_2$ at (j) 6 mm/s and (k) 8 mm/s needle speed; plot of (l) strand printability into 50, 100 and 150 mM $CaCl_2$ at various needle speed and (m) pore printability into 50, 100 and 150 mM $CaCl_2$ at various needle speed.

solution demonstrated reasonable printability (~1 ± 0.1).

3.3. Printability into ionic crosslinker

Although 30 kPa extrusion pressure and 18 mm/s needle translation speed have been identified as the ideal parameters for printing 3D pattern in the 50 mM $CaCl_2$ solution, printing the pattern in an elevated concentration of $CaCl_2$ solution requires further adjustments of the extrusion pressure and needle translation speed. It has been observed that 2% (w/v) composite PCSA precursor is printable in 50, 100, and 150 mM $CaCl_2$ solution only at 20 kPa extrusion pressure and 6–12 mm/s needle translation speed. Accordingly, to assess the strand and pore printability of the composite PCSA precursor in the three different concentration of $CaCl_2$ solution, 20 kPa extrusion pressure and 6, 8, 10, and 12 mm/s needle translation speeds were used as the printing parameter for strand fabrication.

In this section, the printability of composite PCSA precursor extruded into three different concentration of $CaCl_2$ (50, 100, and 150 mM) was evaluated by measuring pore shape and strand width and using formulas (1) and (2). Experimental results show that both the concentration of $CaCl_2$ and the needle translation speed affect the pore geometry and strand width in the biofabrication process for a given extrusion pressure (Fig. 4(l, m)). In particular, strand widths were seen to reduce as a result of an increase in the needle translation speed and changes in $CaCl_2$ concentration (Fig. 4(f–k)).

When the alginate solution was extruded into 50 mM $CaCl_2$, it demonstrated reasonable strand printability (~0.9–0.95) compared to both 100 and 150 mM $CaCl_2$. Bioprinting the alginate precursor into 100 mM $CaCl_2$ with a needle translation speed below 6 mm/s might enhance the strand printability. However, biofabrication of large tissue constructs at lower speeds is time-consuming, and thus the viability of the incorporated cell population might be significantly compromised due to a prolonged time with no growth media. Biofabrication of alginate precursor in a 150 mM $CaCl_2$ solution seemed possible for only 6 and 8 mm/s needle translation speed. Below this limit, the extruded alginate solution was found to gel around the needle before settling down on the printing plate due to the rapid crosslinking property of the $CaCl_2$ solution.

The concentration of the $CaCl_2$ solution also affects the pore shape of the double-layered alginate scaffolds. $CaCl_2$ at different concentrations influences the dimensional uniformity of the extruded strands and thus affect the pore geometry. Of the three concentrations of ionic crosslinkers, 50 mM $CaCl_2$ facilitated the best printability ~ (0.95–1) of porous structures.

3.4. Evaluation of mechanical stability

To evaluate the changes in the mechanical performance of RGD and YIGSR peptide conjugated 2% (w/v) SA scaffolds in the physiologically relevant environment swelling, degradation and compression assessments were conducted in this section. The associated plots were presented in Fig. 5(a–c). All of the composite PCSA scaffolds swelled and lost porous structure over 21 day incubation period when immersed in 10 mM PBS solution (Fig. 5(d)). The percentage of scaffold swelling after 1, 2, 3, and 24 h were measured as 470.9 ± 24.2, 515.7 ± 22.07, 539.6 ± 17.86, and 584.4 ± 15.06, respectively. The data suggest that remarkable swelling took place in the first hour, and then the scaffolds swelled at a slower rate until hour 24. The swelling percentage started to fall at 48 h (551.7 ± 17.43) and declined radically between hours 48 and 168 (551.7±17.43 and 397.9±23.82, respectively). The swelling rate between hours 24 to 48 and hours 168 to 336 seems to be identical but opposite in magnitude, probably indicating the saturation and drop of scaffold degradation, while the rapid loss of swelling rate between hours 48 to 168 suggests severe surface and bulk degradation of the scaffolds. The swelling graph in Fig. 5(a) further demonstrates that significant change in swelling took place between hours 1 to 3 and hours 3 to 24, and hours 48 to 168.

The percentage of weight loss of the scaffolds at day 3, 7, 14, and 21 was calculated as 10.45 ± 3.746, 18.33 ± 2.665, 40.64 ± 6.777, and 52.63 ± 3.689, respectively. The degradation of scaffolds over time has been presented graphically in Fig. 5(b). The degradation of the scaffolds from day 3–7 and day 14–21 seem to happen approximately at the same rate, while the degradation of the scaffolds between days 7–14 occurred at an accelerated rate. However, between day 3–7 and 7 to 14, statistically significant degradation took place. In particular, all the scaffolds lost approximately 20%, 40%, and 55% of their initial mass after 1, 2, and 3 weeks, respectively, when incubated in PBS.

The compression modulus was assessed over 3 weeks after incubating the scaffolds in PBS and is presented graphically in Fig. 5(c). The Young's modulus was measured as 40.3 ± 2.227, 23.7 ± 3.494, 14.67 ± 3.587, and 14.47 ± 2.744 kPa at day 0 (i.e. immediately after fabrication), 7, 14, and 21, respectively. All the scaffolds seem to lose Young's modulus at a rapid rate between day 0–7, then the rate slowed down a bit between day 7–14, and finally reached equilibrium between day 14–21. The biofabricated scaffolds lost ~50% of their Young's modulus in the first week, and an additional ~20% of their Young's modulus by the following week while incubating in PBS. Statistical analyses suggest that scaffolds lost elastic modulus significantly between days 0–7 and days 7–14.

3.5. Evaluation of surface morphology

Surface morphology of RGD and YIGSR peptide conjugated 2% (w/v) SA scaffolds incubated in PBS was assessed with SEM images (Fig. 5(e–g)). The Fig. 5(e–g) demonstrates macro- and microscale changes on the surface of the composite PCSA strands over a period of 3 weeks of incubation. The images demonstrated that over time, the strand surface became micro-porous probably due to the effect of surface and bulk degradation. Interestingly, the biofabricated pores were still evident in the scaffolds after 3 weeks of incubation in PBS. However, structural integrity seems to have been compromised over the incubation period.

3.6. Assessments of RPSCs morphology in 2D culture

Cell morphology was studied on prepared 2D surfaces for positive control, negative control, and experimental groups using PLL, SA, and PCSA hydrogel coatings, respectively, on round coverslips which are shown in Fig. 6(a). During the culture period, most of the RPSCs seeded on the SA surface maintained circular morphology and formed clusters (Fig. 6(c)). In contrast, RPSCs did not form clusters on PLL (Fig. 6(b)) and PCSA (Fig. 6(d–f)) surfaces, rather the cells started to spread over the 2D surface, attached well to the polymer, and developed elongated morphology. Notably, RPSCs cultured on single-PCSA-coated surfaces showed a small number of cells with unipolar, bipolar, and multipolar morphology. In contrast, RPSCs cultured on PLL- or composite PCSA-coated surfaces showed a significant number of cells with unipolar, bipolar, and a multipolar morphology. Measuring the response of RPSCs to the peptide-modified alginate demonstrated that the modified alginate was superior in promoting suitable cell morphology over unmodified alginate, and these results are shown in Fig. 6(g–i). The number of attached cells per 0.06 mm^2 on the composite PCSA surface was 80.33 ± 8.96, which was close to the attached cell population (i.e. 89.67 ± 4.73) on the positive control. YIGSR-alginate conjugate (YCSA) supported a higher number of cell (80 ± 4) attachment compared to that of RGD-alginate conjugate (RCSA) surface (73.33 ± 4.16). Accordingly, cell attachment on the composite PCSA, YCSA, and RCSA surface was significantly higher than the negative control. Interestingly, of the three experimental groups, cell attachment was significantly low on RCSA surface related to the positive control.

The cell circularity measured on the RCSA, YCSA, and composite PCSA surface were 0.54 ± 0.04, 0.8333 ± 0.06, and 0.4333 ± 0.08, respectively, which was significantly lower than the negative control (0.9733 ± 0.02). The cell circularity value was significantly higher on

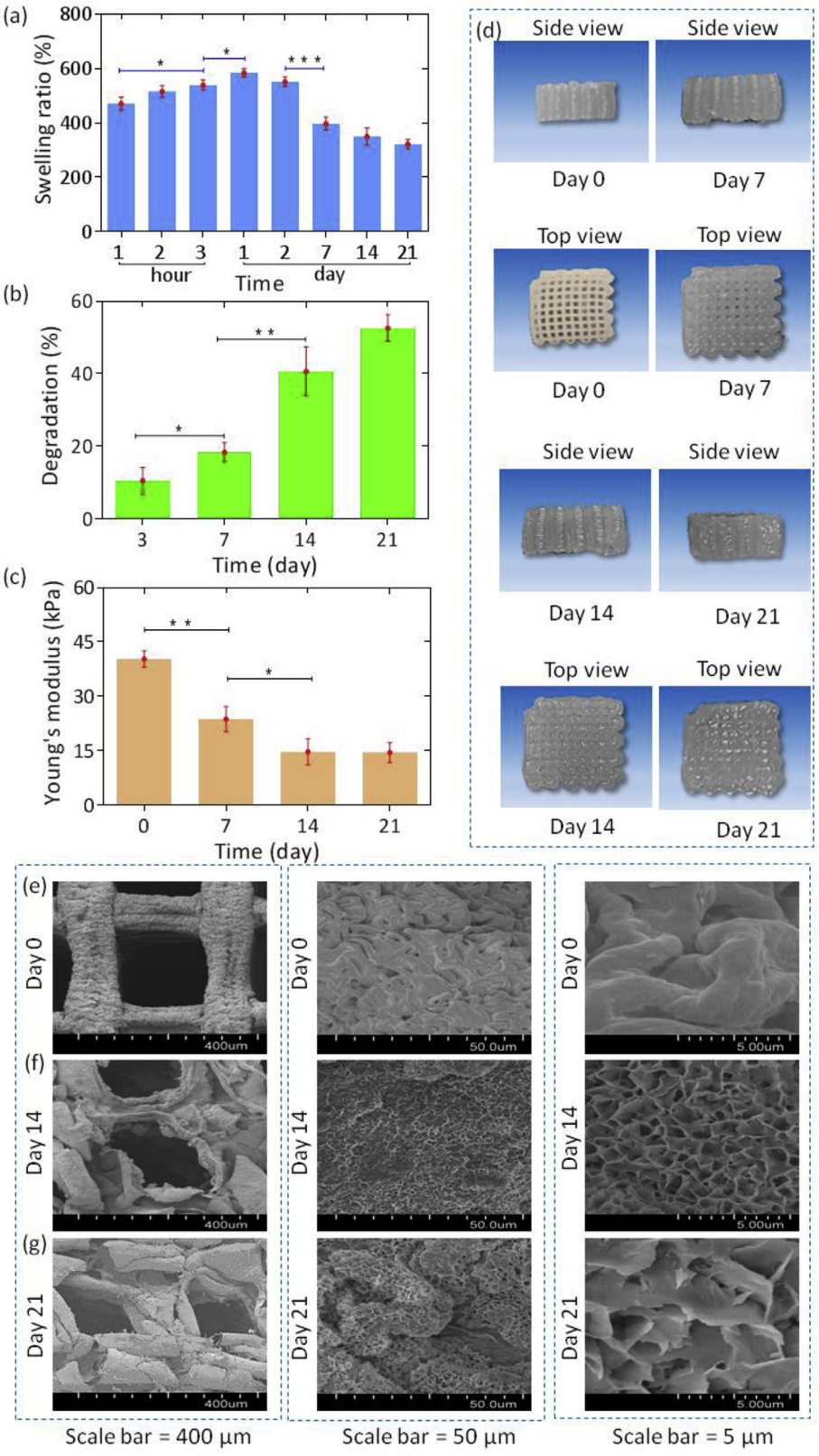

Fig. 5. Assessment of mechanical stability and surface morphology of RGD/YIGSR-alginate conjugate scaffolds after PBS incubation at predetermined time points: (a) swelling ratio, (b) degradation percentage, (c) Young's modulus, (d) macroscopic view of scaffolds at day 0, 7, 14, and 21, and SEM images of scaffolds at (e) day 0, (f) day 14, and (g) day 21, and from left to right images with higher magnification have been presented.

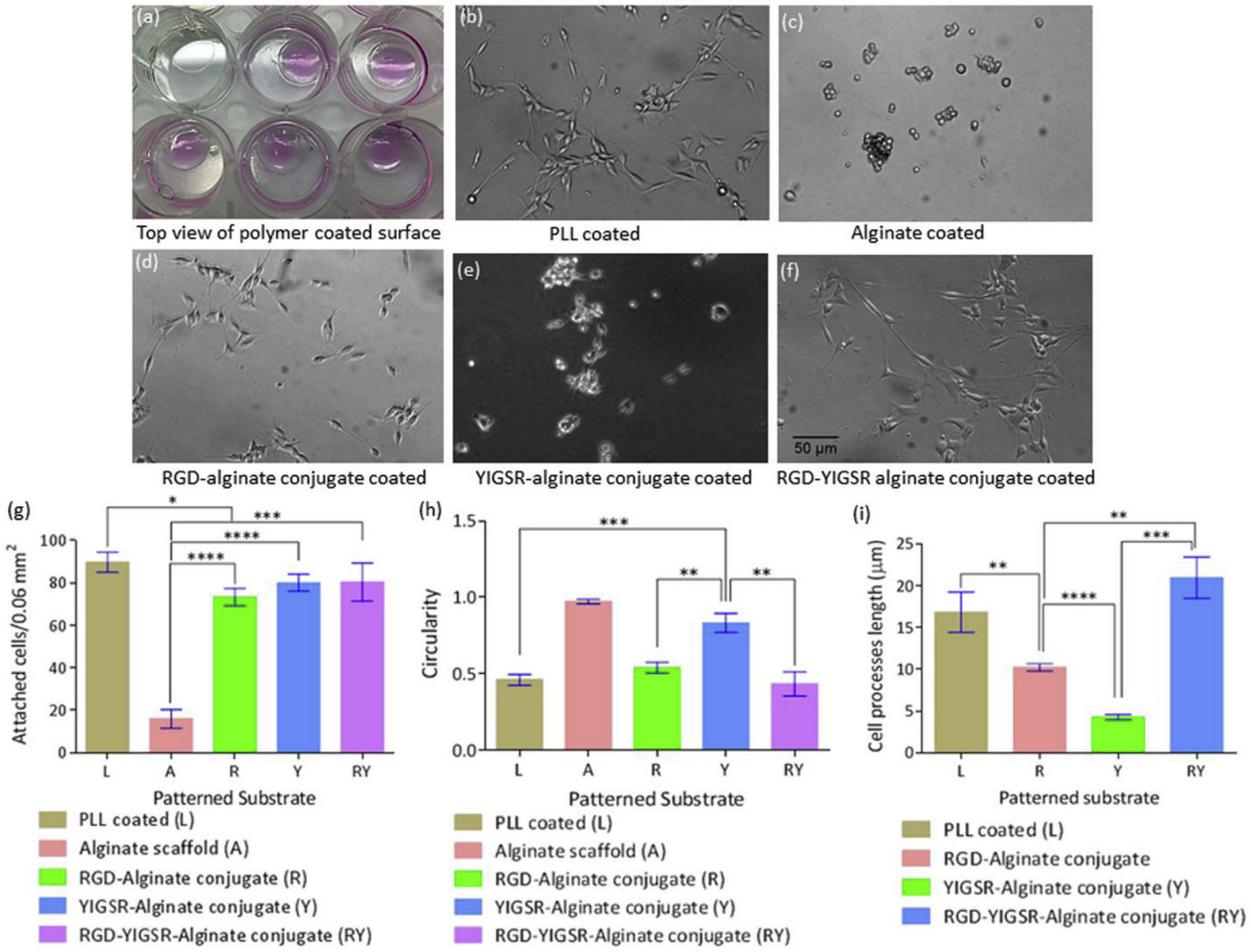

Fig. 6. 2D culture of primary rat Schwann cells on various polymer-coated round coverslips for 3 days; (a) top view of cells growing on polymer-coated coverslips in a tissue culture plate after 3 days of culture; microscopic images of RPSCs grown on (b) PLL coated, (c) alginate coated, (d) RGD-alginate conjugate coated, (e) YIGSR-alginate conjugate coated, and (f) RGD-YIGSR-alginate conjugate-coated surface; plots of (g) number of attached cells, (h) circularity of the adherent cells, and (i) length of cell processes on different polymer coated 2D surfaces (Scale bar (b–e) = 50 µm; *p < 0.05, **p < 0.01, ***p < 0.001, ****p < 0.0001).

YCSA surface compared to RCSA, composite PCSA, or PLL coated surface (0.46 ± 0.04). Notably, RPSCs showed identical morphology on composite PCSA surface and positive control. The cell processes grew on RCSA and YCSA surface were 10.23 ± 0.454 and 4.277 ± 0.323 µm, respectively, which were shorter than the processes grown on positive control (16.82 ± 2.396 µm). Statistically, the length of cell processes on YCSA surface was significantly shorter than both the RCSA and the composite PCSA surface (20.95 ± 2.481 µm). Remarkably, RPSCs cultured on the composite PCSA surface grew longer processes than positive control and significantly longer than RCSA surface. As Schwann cells did not develop processes in unmodified alginate, this substrate is not included in Fig. 6 (i).

3.7. Assessments of RPSCs viability in 3D culture

The cellular biocompatibility of the substrate is important for ensuring cell viability. The cell viability assay results are illustrated in Fig. 7. Again, unmodified alginate was generally inferior to the other substrates, and cells often grew in clumps. RCSA strands showed favorable cell viability (90.71 ± 2.89) at day 0 but had decreased (80.81 ± 5.547) by day 3, and this trend continued (85.05 ± 5.12) on day 7. RCSA strands also had RPSCs growing in clumps, though not as frequently nor as large as unmodified alginate, and had a similar, even distribution of dead cells as unmodified alginate. At day 0, 3, and, 7, the percentage of RPSCs viability in the YCSA strands was measured as 91.74 ± 3.193, 87.33 ± 4.14, and 89.47 ± 3.644, while in the composite PCSA strands was measured as 94.9 ± 0.7851, 90.63 ± 6.06, and 95.01 ± 1.954, respectively. It is obvious that RPSCs viability decreased in all experimental samples at day 3, suggesting there might be extrusion-induced cell damage or cell apoptosis in the PCSA hydrogel due to the leftover toxic byproducts of the conjugate reaction. Over time the toxins might diffuse out from the hydrogel and enhance the viability of RPSCs. The hydrogel strands showed enhanced RPSCs viability at day 7 compared to day 3, suggesting both self-healing and proliferation of the cells. Fig. 7(i–k) reveals that YCSA strands showed comparable results to composite PCSA throughout the seven days. The result also suggests a combined effect of composite peptides over a single peptide-alginate conjugate. However, single and composite peptide-alginate conjugate, though close in comparison, were inferior to the positive control (PLL-coated plate) and superior to the negative control (alginate) in the 7-day culture period. Moreover, experimental results indicated that RPSCs viability among the peptide-alginate conjugates was statistically insignificant at day 0 and 3, while cell viability in the composite PCSA strands was significantly different from RCSA strands at day 7. RPSCs viability in

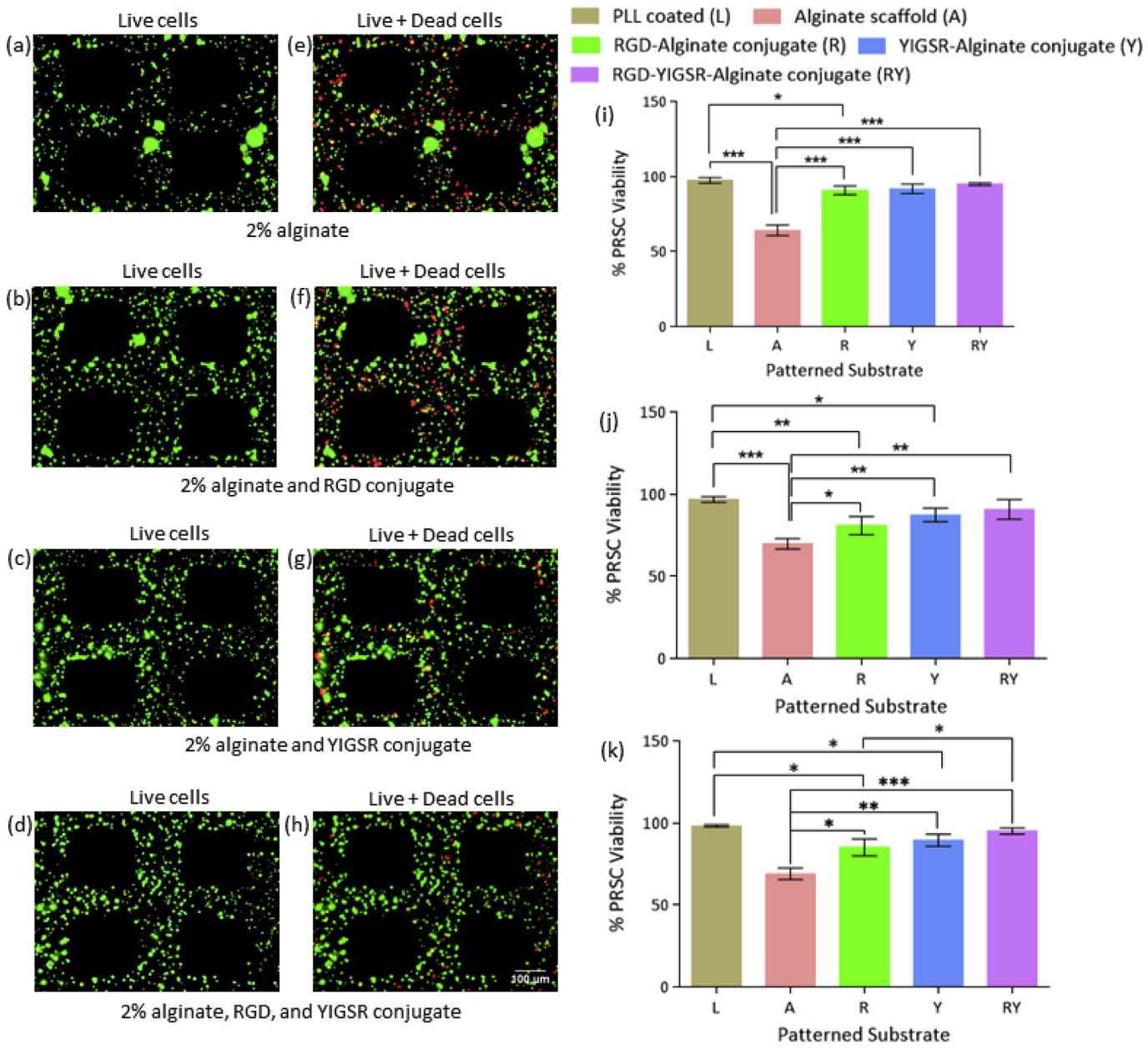

Fig. 7. Primary Schwann cell viability in bioplotted strands after 7 days of 3D culture where live and dead cell stains as green and red, respectively; live cells in (a) 2% alginate, (b) 2% alginate –RGD conjugate, (c) 2% alginate –YIGSR conjugate, (d) 2% alginate –RGD-YIGSR conjugate; live and dead cells in (e) 2% alginate, (f) 2% alginate –RGD conjugate, (g) 2% alginate –YIGSR conjugate, (h) 2% alginate –RGD-YIGSR conjugate (scale bar = 100 µm); cell viability graphs for (i) day 0, (j) day 3, and (k) day 7 (*$p < 0.05$, **$p < 0.01$). (For interpretation of the references to color in this figure legend, the reader is referred to the Web version of this article.)

the alginate strands was significantly low compared to the peptide alginate conjugates and the PLL-coated plate over the culture period. Moreover, cell viability in the PLL-coated plate was significantly greater than RCSA strands over the 7-day culture period and YCSA strands at day 3 and 7.

3.8. Cell-biopolymer interactions in 3D culture

Three-dimensional printing creates an environment that embedded cells can respond to in a way that better mimics *in vivo* environments. Fig. 8(c–g) shows both the images of the cell processes that developed and the quantification of how long the cell processes were. RPSCs are seen to distribute uniformly in the RCSA, YCSA, and composite PCSA strands. As with the 2D culture, RPSCs grew unipolar, bipolar, and multipolar processes in the hydrogel. In the peptide-alginate conjugate, cell processes combined together to promote cell-cell interaction. Culturing RPSCs in RCSA strands resulted in longer cell processes (21.54 ± 1.115 µm) than YCSA strands (14.12 ± 1.244 µm), which is similar to the results from 2D culture (Fig. 6(i)). Similar to 2D culture, the cell processes that developed in RCSA strands were shorter in length than those in composite PCSA strands (24.48 ± 1.047 µm). Notably, the cell processes grew in YCSA strands were significantly shorter than RCSA or composite PCSA strands. Likewise, statistically significant cell process difference was observed in the RCSA and composite PCSA strands. In contrast, most RPSCs embedded in the alginate hydrogel showed circular morphology, and though cell processes did develop in the alginate cell culture, the processes (5.57 ± 1.157 µm) were much shorter than the modified alginate cell cultures.

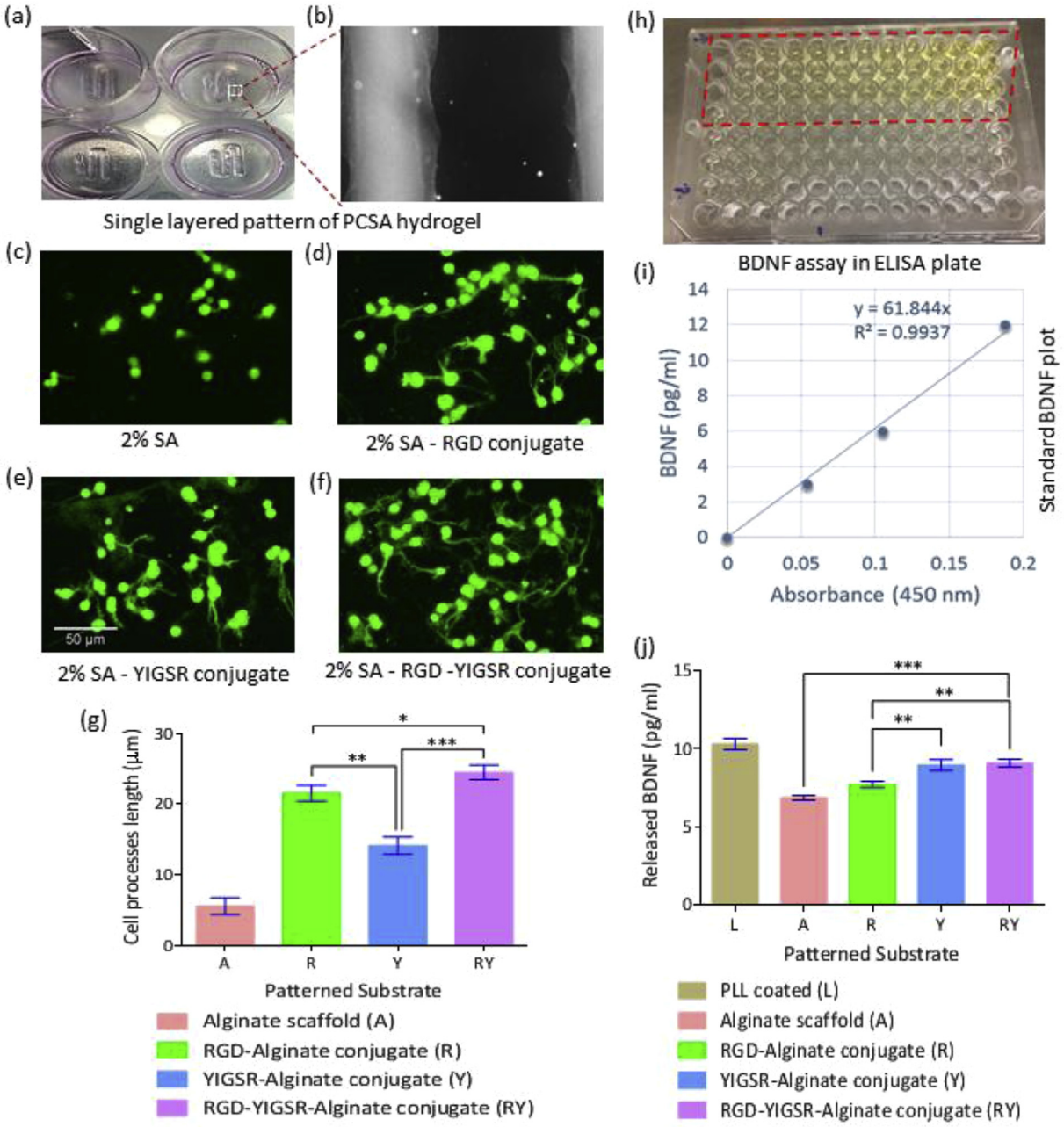

Fig. 8. Assessments of 3D culture of RPSCs and released BDNF in and from the bioprinted hydrogel strands with immunofluorescence assay and ELISA kit, respectively; (a and b) single layered patterns; S-100 immunocytochemistry (green) on RPSCs for 3D cultures grown in (c) alginate, (d) RGD-modified alginate, (e) YIGSR-modified alginate, and (f) RGD-YIGSR-modified alginate strands. [*$p < 0.05$, **$p < 0.01$, ***$p < 0.001$]. (g) Graphical presentation of cell processes length; (h) yellow solution in the wells of ELISA plate indicating the amount of released BDNF, (i) standard BDNF plot, (j) secreted BDNF [**$p < 0.01$, ***$p < 0.001$]. (For interpretation of the references to color in this figure legend, the reader is referred to the Web version of this article.)

3.9. Assessments of BDNF secretion

To evaluate the physiological function of RPSCs in 3D culture after 3 days, the level of BDNF was quantified using an ELISA assay. The graded distribution of yellow color in the ELISA plate demonstrate the varying amount of secreted BDNF by the embedded RPSCs in the hydrogel (Fig. 8(h)). From the sequential dilution of standard BDNF in the ELISA plate, the correlation between the known amount of BDNF and light absorbance was developed in order to calculate the amount of secreted BDNF by experimental samples (Fig. 8(i)). All RPSCs cultures showed a release of BDNF. In similarity to the previously-discussed experiments, cultures in alginate released the least amount of BDNF (6.847 ± 0.14 pg/ml), and cultures in RCSA hydrogel showed lower levels of BDNF (7.71 ± 0.19 pg/ml) release compared to YCSA and composite PCSA hydrogel, which was 8.943 ± 0.36 and 9.067 ± 0.25 pg/ml, respectively. Moreover, the amount of BDNF secreted by the RPSCs embedded in RCSA hydrogel was significantly lower than in YCSA and composite PCSA hydrogel. Interestingly, RPSCs embedded in YCSA and composite PCSA hydrogel had very similar levels of BDNF (Fig. 8(j)), which is in contrast to the length of the processes that developed in the 3D culture assay (Fig. 8(g)). Compared to the PLL-coated plate that served as a control, all of the modified alginate showed lower levels of BDNF release.

3.10. Evaluation of protein expression of RPSC

As neurons regenerate, they respond to cues in their environment,

and that includes Schwann cells. In Fig. 9, immunocytochemistry images are shown of developing neurons from cells seeded on a 2D culture surface that was embedded with Schwann cells. As mentioned earlier, the neurons were collected from stimulated DRGs of Sprague Dawley rats and seeded on the samples immediately after preparation. In Fig. 9(a–c), the influence of Schwann cells and peptides on helping to support the growth of neurons and axons is visible by the Schwann cells aligning along the axon. In addition, the elongated morphology of the RPSCs in the peptide modified alginate strands has been demonstrated using S-100 immunofluorocytochemistry. Particularly, clusters of RPSCs are found in the close vicinity of neuron cells, suggesting the influence of chemotaxis and cell-cell interactions. DAPI staining highlights all of the nuclei of RPSCs and neuron cells in the hydrogel strands, demonstrating that RPSCs are found more uniformly distributed in the RCSA strands compared to YCSA or composite PCSA strands. Using β-3 immunofluorocytochemistry to selectively stain neurons demonstrated that neurons grew neurites in different directions on the peptide-modified alginate surface. Since neuron cells were seeded on the PCSA strands bioprinted in the 0° direction (Fig. 12(f)), the neuron cells should grow their neurites in the same direction due to the presence of physical and biochemical cues [29]. Notably, a higher number of neurites were found aligned with the direction of 3D printing that were grown on the RCSA or composite PCSA strands than on the YCSA strands. However, neuron cells were found to grow tiny neurites on the alginate strands (i.e. negative control), the images of immunocytochemistry were presented in Fig. 9 (d). The growth of neurites on the PLL-coated plate (i.e. positive control) was also investigated and presented in Fig. 9 (e). The neurites were seen to grow in different directions and coil around neuron cell body on the PLL coated plate.

The 3D orientation of RPSCs, neurons, and neurites has been presented for single or composite peptide alginate conjugate strands (Fig. 10(a–c)). The images clearly demonstrate the geometry of bioprinted strands and the directional developments of neurites on the patterned substrate. The Fig. 10(a–c) demonstrate that most of the neurites grew on the outer surface of the PCSA strands.

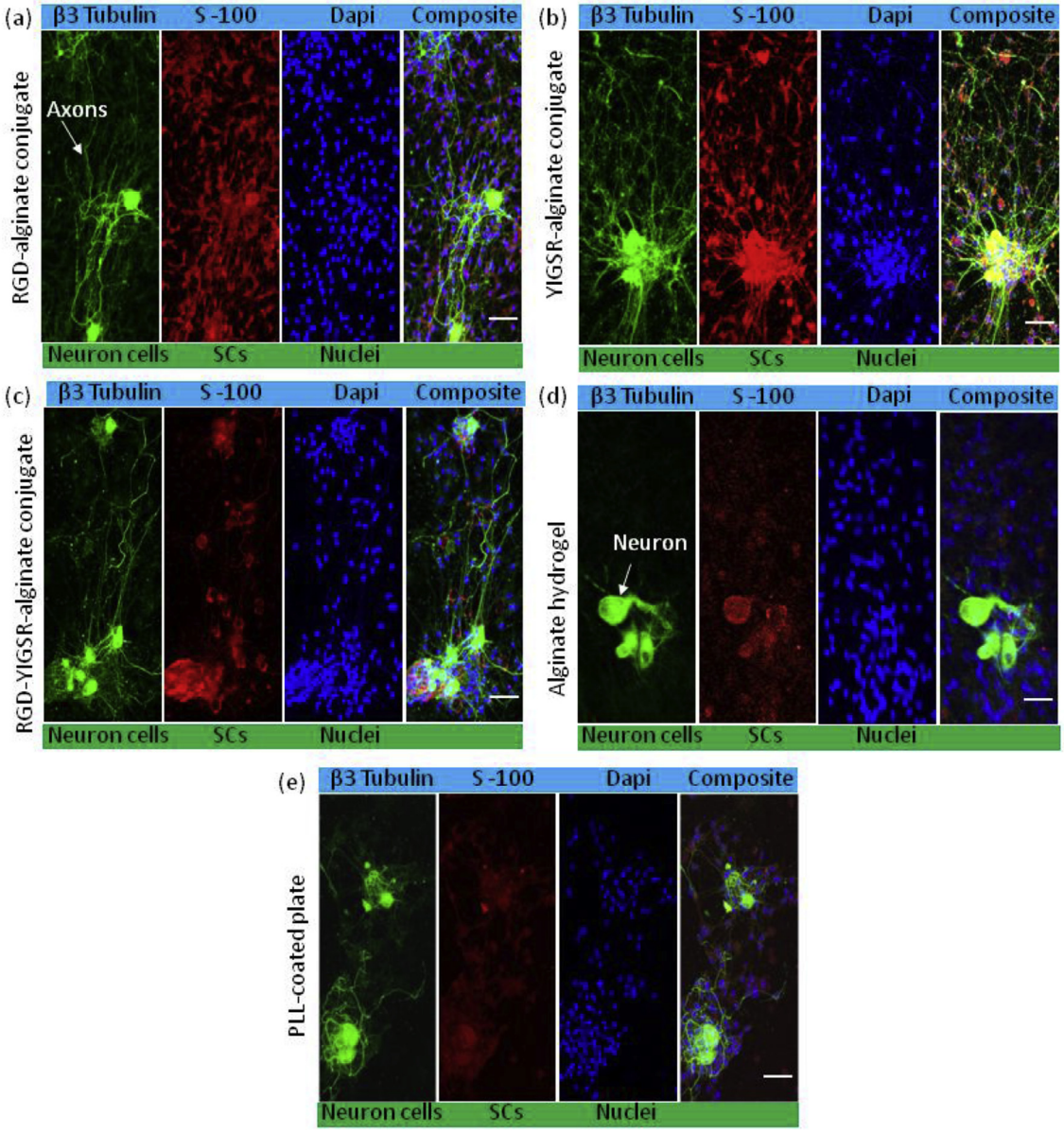

Fig. 9. β-3 tubulin immunocytochemistry (green) and S-100 immunocytochemistry (red) on neuron cells and Schwann cells, respectively with DAPI staining (blue) of nuclei for cultures grown on (a) RGD-alginate conjugate, (b) YIGSR-alginate conjugate, (c) RGD-YIGSR-alginate conjugate strands, (d) alginate hydrogel, and (e) PLL-coated plate; [scale bar = 100 μm]. (For interpretation of the references to color in this figure legend, the reader is referred to the Web version of this article.)

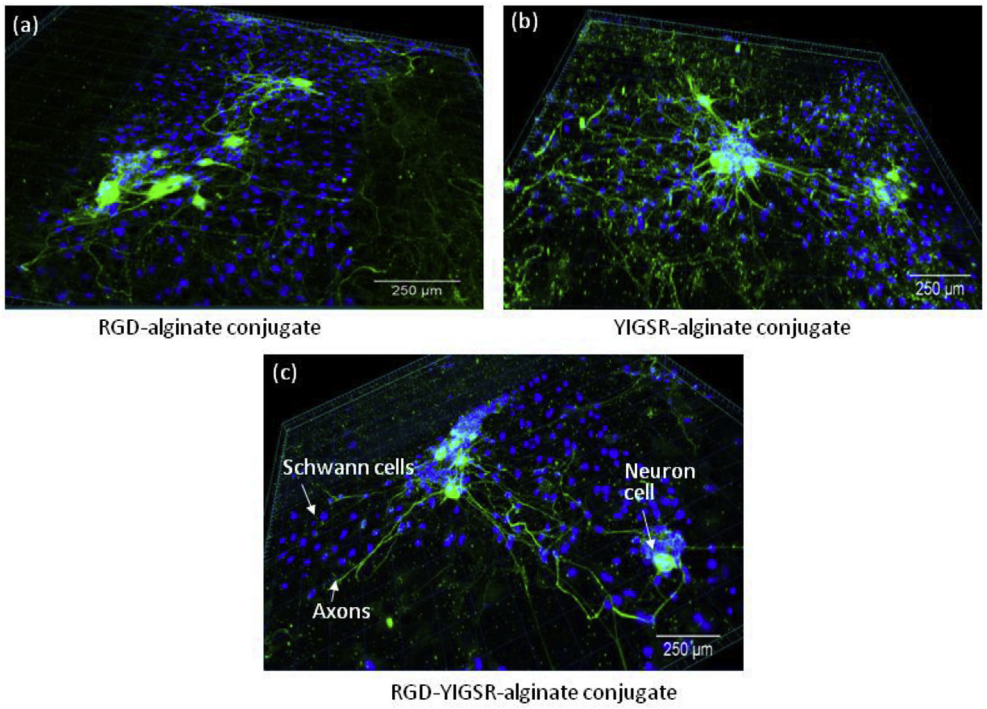

Fig. 10. Confocal microscopy of neuron and Schwann cells distributed three-dimensionally in the (a) RGD-alginate conjugate, (b) YIGSR-alginate conjugate, and (c) RGD-YIGSR-alginate conjugate; β-3 tubulin immunocytochemistry (green) on neuron cells with DAPI staining (blue) of nuclei both for neuron and primary Schwann cells; [scale bar = 250 μm]. (For interpretation of the references to color in this figure legend, the reader is referred to the Web version of this article.)

3.11. Evaluation of length and directional growth of neurites

Fig. 11 highlights the growth of axons from neuron cells along the strand of the scaffold. In combination, these five figures demonstrate the combined effect of biopolymer, Schwann cells and neurons in culture on the directional growth of axons. Analogous to the effects of conjugated peptides on the growth of cell processes of Schwann cells, the length of the neurites that develop is dependent on the peptides that were used. The composite PCSA promoted outstanding neurite growth (1548.2 ± 126.4 μm), and the neurite length on RCSA strand (1404.1 ± 361.2 μm) was superior to YCSA strand (926.8 ± 41.4 μm) or PLL coated plate (639.0 ± 103.9 μm) or alginate strand (238.0 ± 64.5 μm). Interestingly, neurite length on the PLL-coated plate was found shorter than the PCSA strands. This further highlights the probable influence of peptides and Schwann cells in helping to guide and support the growth of neurites.

Three-dimensional printing can create microstructures that embedded cells can respond to and potentially stimulate the directional growth of cell processes. The addition of compounds, such as the peptides that were conjugated to the alginate in this experiment, can influence the ability for RPSCs to respond to those cues. The directional distribution of neurites has been evaluated by frequency versus angular orientation (Fig. 12(a–e)). The strands were fabricated in the direction of 0°, and a significant number of neurites have been seen to align in the $0° \pm 30°$ direction, though for all three peptide-alginate conjugates, neurite growth was observed in the (75° to 90°) or (−75° to −90°) direction as well, which suggests the probable growth of some misguided neurites perpendicular to the strand towards culture plate. The fact that the majority of the neurites grew parallel to the strand in all three PCSA samples suggests the dominant effect of peptides possibly aligned along the 0° direction. The most consistent directional growth of neurites along the longitudinal axis was on the composite PCSA strands, with a frequency of ~0.08 for the direction of neurite extension. Notably, the YCSA strands failed to facilitate consistent directional neurite growth of all three experimental samples, since the maximum value of frequency was found on both 0 and 90° directions. Likewise, the alginate strands and PLL coated plate failed to grow a greater part of neurites along $0° \pm 30°$ direction, rather both the controls grew neurons randomly between 0 and 90° directions.

4. Discussions

In extrusion-based 3D printing, the printability of hydrogel precursor largely depends on the viscosity of the precursor. The high viscous hydrogel precursor required higher extrusion pressure, while the very low viscous hydrogel precursor freely dripped from needle due to gravity (i.e. without any pneumatic pressure) [30]. Furthermore, biofabrication of scaffolds using hydrogel precursor in an ionic crosslinker might require higher extrusion pressures compared to dispensing in air if the crosslinker exhibits a rapid gelation rate. Particularly, at low dispensing pressures, the hydrogel precursor might often get crosslinked around the needle opening prior to settling on the fabrication plate. At a particular pressure, adjusting of the needle or stage speed to faster or slower might result in the fabrication of hydrogel strands that will most closely match the theoretical values [31]. Unfortunately, biofabrication with the alginate precursor in the ionic crosslinker did not allow for a wide range of needle speeds. For this reason, only a few needle speeds were investigated in this article.

Several factors caused the deviation of experimental results from the theoretical values (e.g. strand width, pore shape, and angle formations). Any mismatch between extrusion pressure, needle speed, and gelation rate might result in poor printability. In particular, inconsistency between the biopolymer flow rate and needle translation speed might lead to rupture and tearing due to under extrusion or random coiling. It is because of the over extrusion of the biopolymer strand prior to settling down and adhering to the plate. There might be no enough time for crosslinking resulting in poorly formed scaffolds as well, as another reason. Notably, PEI-coated tissue culture plates were used in this study to allow the extruded strands to adhere to the plate and in their predefined geometry. At higher linear speeds, the extruded strands start

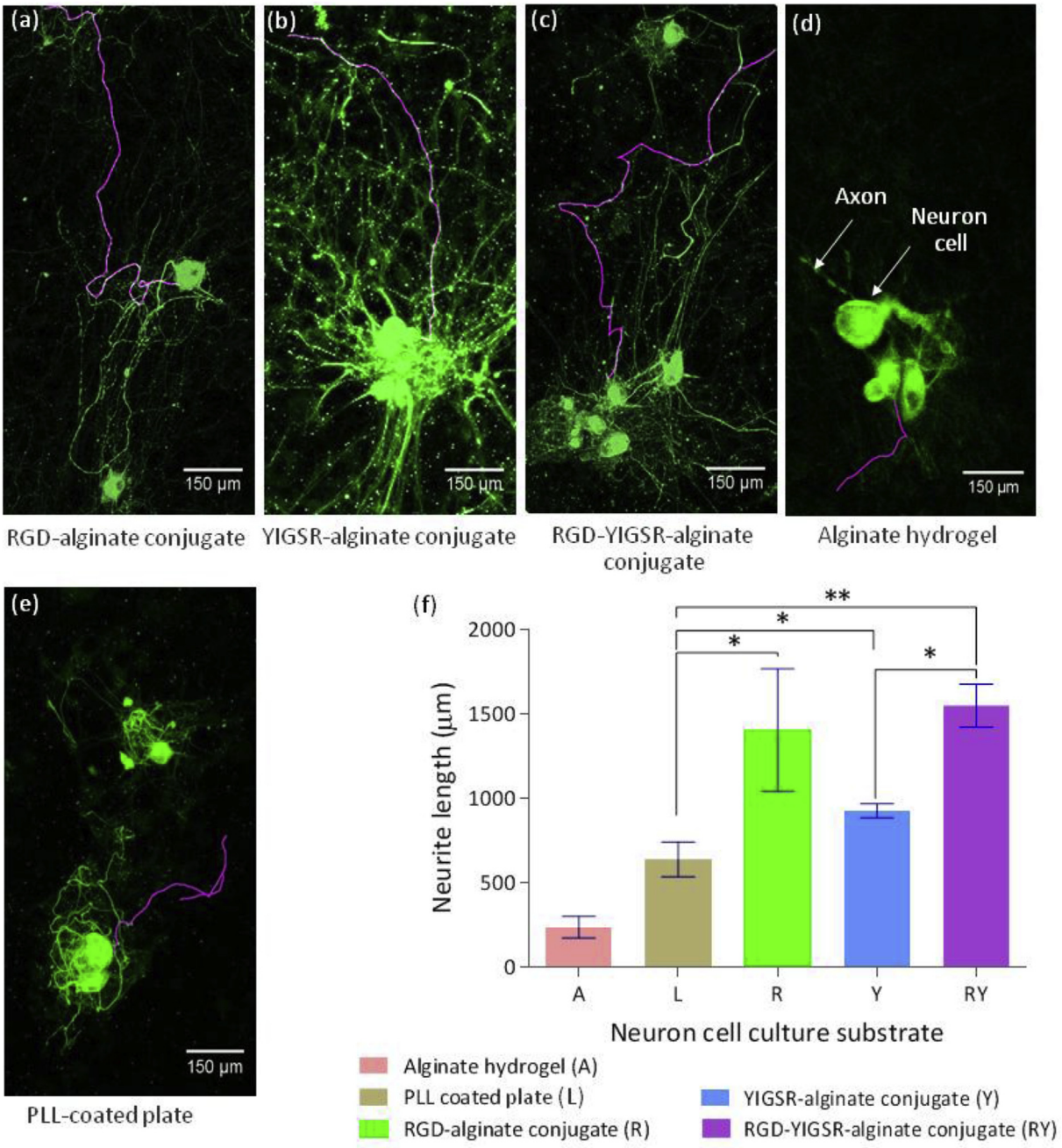

Fig. 11. Outgrowth of neurites cultured on single layered scaffolds fabricated with (a) RGD-alginate conjugate, (b) YIGSR-alginate conjugate, (c) RGD-YIGSR-alginate conjugate, and (d) alginate hydrogel. Neuron cells cultured on (e) PLL-coated plate was considered as positive control, (pink color demonstrates the directional pathway of neurites) [*$p < 0.05$, **$p < 0.01$]. (For interpretation of the references to color in this figure legend, the reader is referred to the Web version of this article.)

floating in the crosslinking solution instead of settling down due to the incongruity between gelation rate, surface attachment, and buoyancy force. This suggests that there exists a limit for the minimum and maximum linear speed for a particular needle opening with respect to biopolymer viscosity and extrusion pressure. Below and above the limit, the hydrogel precursor demonstrates poor printability. Accordingly, for three extrusion pressures and a particular needle opening, a number of linear needle speeds were identified in this study that caused moderate to outstanding printability of composite PCSA precursor.

For all measurements, the second layers were chosen as the layer to evaluate to eliminate the polymer spreading generated by the surface tension on the printing surface. A nonuniformity in the strand width along the length of the stand was seen due to the spreading and fusion of the second layer with the previous layer where they intersect. This phenomenon resulted in under printability ($\sim P^{<}1$) at the intersections and between intersections for the strands fabricated with 20 or 30 kPa extrusion pressure for particular needle speeds. In contrast, for 40 kPa extrusion pressure, over printability ($\sim P > 1$) at the intersections and between intersections was observed due to excess hydrogel deposition with respect to different needle speeds. Moreover, the concentration of $CaCl_2$ also affected the strand and pore printability. In crosslinking the extruded strands, Ca^{2+} ions enter between the molecular chains of alginate monomers and form intermolecular ionic bonds, which induces a sol-gel transition. Using $CaCl_2$ at higher concentration supplies more Ca^{2+} ions to the extruded alginate precursors and promotes fast reaction kinetics. Consequently, in this study it was noticed that strand fabrication

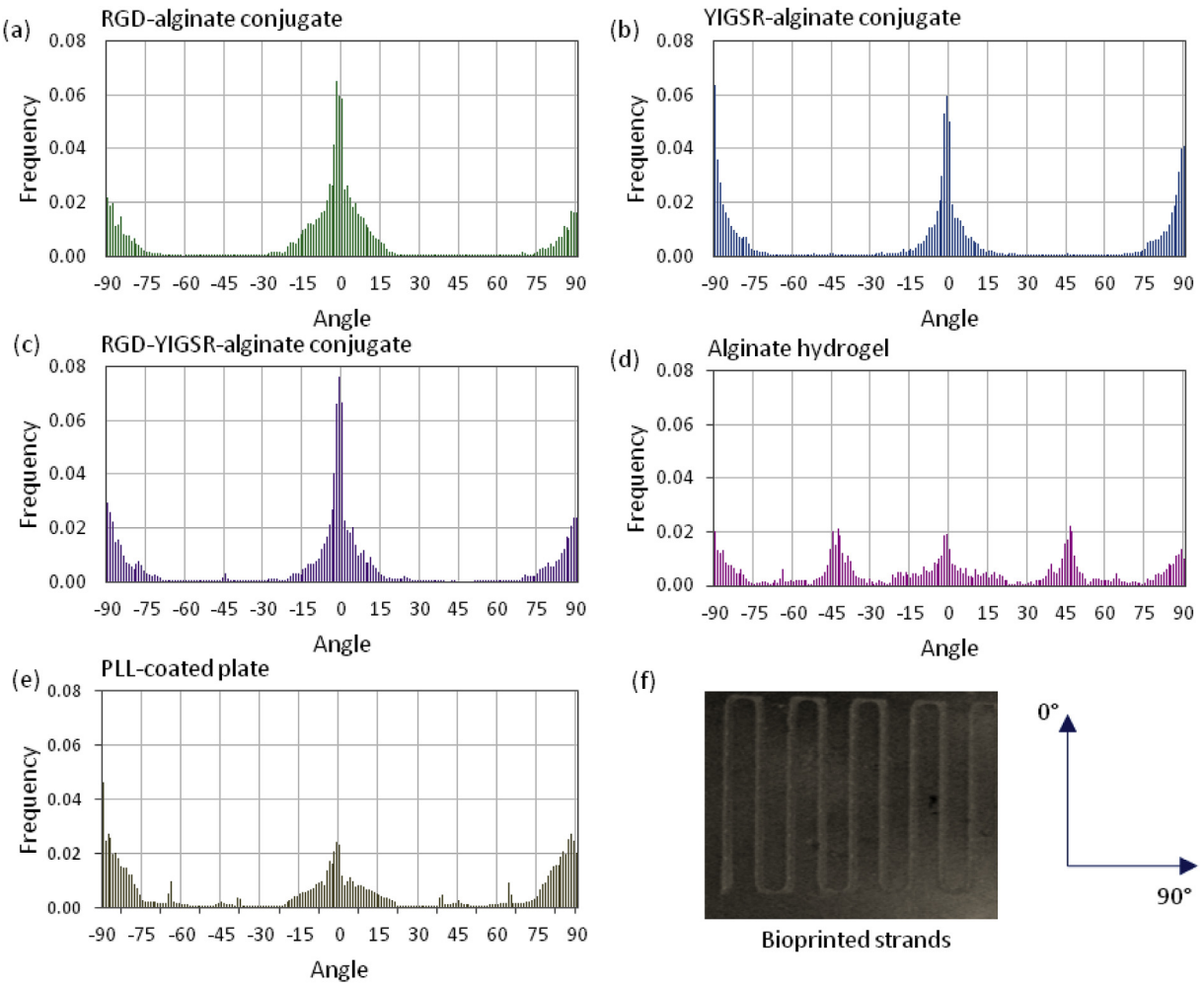

Fig. 12. 2D distribution of neurites grown on single layered patterns fabricated with (a) RGD-alginate conjugate, (b) YIGSR-alginate conjugate, (c) RGD-YIGSR-alginate conjugate, and (d) alginate hydrogel. Neuron cells cultured on (e) PLL-coated plate was considered as positive control and (f) single layered scaffold showing 0° and 90° direction.

was possible only at lower needle speeds (i.e. 6 and 8 mm/s) in the elevated concentration of $CaCl_2$ solution (i.e. 150 mM). The invasion of more Ca^{2+} ions into molecular structure cause shrinkage, which is obvious in the experimental results. Thus, the shrinkage of composite PCSA precursor caused inferior strand and pore printability at elevated concentrations of $CaCl_2$ (i.e. 100 and 150 mM).

Swelling, degradation, and loss of Young's modulus of the alginate scaffolds could be attributed to ion exchange, polymer chain relaxation, and water uptake mechanism. The ion exchange (Ca^{2+}/Na^{+}) between hydrogel and PBS solution probably relaxes the bond between polymeric chains inside hydrogel and facilitates the water uptake mechanism. From the swelling graph (Fig. 5(a)), it is obvious that most of the ion exchange took place in the first 24 h since the incubation was conducted in a fixed volume of PBS. Because the composite PCSA scaffolds started degrading along with swelling over time, the swelling of the scaffolds was found to decline after day 1. In particular, mass loss from the scaffolds reduced the value of swelling obtained from equation (4). Similarly, the degradation graph (Fig. 5(b)) demonstrates that probably surface degradation was most prominent in the first week, while primarily bulk degradation and polymer dissolution likely took place in the following weeks. However, the lack of ion exchange slowed down the degradation process in the third week. Since both swelling and degradation affect the Young's modulus of the bioprinted scaffolds, the scaffolds lost 70% of initial elastic modulus within the first two weeks of incubation.

The changes to the surface morphology of the composite PCSA scaffold over time has profound effects on tissue growth, particularly for nerve tissue regeneration. Since the strand surface became micro-porous over time, the scaffolds seem to be conducive for mass diffusion exchange between the incorporated cell populations and the surrounding fluids [28]. Moreover, the extended incubation period increased the roughness of the composite PCSA scaffold, which could have an influential effect on nerve regeneration [32]. The alginate scaffolds investigated in this study contain both biochemical (i.e. conjugated peptides) and biophysical (i.e. surface roughness) cues required for axon outgrowth. In nerve tissue regeneration, the micro-porous scaffolds might ensure reasonable viability of incorporated Schwann cells and facilitate neurite growth in a nerve guidance conduit.

Biocompatible alginate has been frequently studied in various tissue engineering application due to its low cytotoxicity and bio-printability. However, alginate hydrogels are unable to regenerate tissue due to the lack of cell-binding peptides in the molecular structure. Since extracellular-matrix-derived RGD and laminin-derived YIGSR peptides bind to integrin and laminin receptors of neuron cells, respectively, co-valent chemistry was used to link RGD and YIGSR peptides to SA monomers in this study to enhance axon growth. Modification of the alginate by individual single peptide-modified alginate showed favorable results, though the results from the composite peptide-modified alginate suggested that there is an interactive effect from their combination. Unmodified alginate generally showed very poor results in promoting cell attachment, morphology, and processes. RCSA was routinely

superior to YCSA hydrogel, though composite PCSA hydrogel was generally superior to the other culture substrates being evaluated. While RGD peptides facilitate cell adhesion and process growth through interacting with integrin receptors, YIGSR peptides promote cell proliferation by interacting with laminin receptors on neuron cells. This was demonstrated where RCSA hydrogel influenced the RPSC cells to show more elongated morphology and grow longer processes compared to YCSA hydrogel, while YCSA hydrogels induced the formation of cell clusters through cell proliferation. RPSCs attached very poorly to unmodified alginate, whereas they attached to the modified alginate culture substrates in comparable numbers to the PLL-coated tissue culture plate that served as a positive control. A sign of favorable RPSC response is the degree of polarity that the cells develop, where the composite PCSA hydrogel was superior to the other culture substrates. Another measure of the cellular polarity is the length of the processes that develops in the cell. Here again, composite PCSA was superior to all other culture substrates, and markedly so compared to the other modified alginates due to the simultaneous interaction of the composite peptides with the two cell receptors.

BDNF, a member of the neurotrophin family, supports the survival, growth, and differentiation of neuron cells. In addition, BDNF stimulates the regeneration of damaged peripheral nerves and the axon remyelination process. In tissue engineering applications, the controlled release of BDNF has been shown to be beneficial for axon regeneration. However, released BDNF has a short half-life and thus will lose bioactivity before axon regeneration is complete. *In vivo*, Schwann cells secrete BDNF after nerve injury that regulate the growth of neurites from neuron cells. Therefore, in this study RPSC were embedded in peptide-alginate conjugates to provide a controlled and continuous release of BDNF and to evaluate the potential for future application in promoting axon regeneration. The amount of BDNF secreted by the RPSC was minimal in this study. The number of incorporated cells in one layer, the amount of taken supernatant, and the leftover BDNF in the hydrogel might cause the small amount in experimental measurements. However, the RPSC embedded in peptide-alginate conjugated strands secreted greater amount of BDNF compared to negative control and smaller amount of BDNF than positive control. In particular, RPSC incorporated in composite PCSA demonstrated superior result of the three experimental samples, suggesting the simultaneous interaction of integrin and laminin receptor on the production of BDNF.

Physical and biochemical cues are essential for guiding neurite growth after PNS injury. To achieve the goal, patterned structures were biofabricated in this study using an alginate bio-ink that has been conjugated with either single or composite peptides. The seeded neuronal cells were seen to grow their neurites on the patterned substrates and responding to the cues in their microenvironment. RPSC seemed to distribute unevenly in the YCSA- and composite PCSA-strands compared to RCSA-strands, suggesting the effect of RGD peptide on cell migration within the biopolymer. The single-layer strands didn't degrade much during the 7-day culture period and maintained their structural integrity. During the culture period, the neuronal cells grew ~1–1.5 mm-long neurites on all three peptide-conjugated alginates, which is quite impressive. Of the five samples studied, composite PCSA strands demonstrated outstanding outcomes in terms of directional neurite growth. Therefore, alginate conjugated with multiple types of peptides should be considered as a potential superior bio-ink for nerve tissue regeneration for future study.

5. Conclusion

In this study, a set of experiments were conducted to characterize PCSA scaffolds in terms of printability, mechanical stability, and neurite outgrowth. Experimental results suggest that the selection of extrusion pressure, needle translation speed, and crosslinker concentration has profound effects on the strand printability of composite PCSA precursor. However, arbitrary selection of these parameters does not facilitate reasonable printability. Using a needle translation speed range of 12–20 mm/s and an extrusion pressure of 30 kPa supported better average strand width printability (~0.9–1) than either 20 or 40 kPa extrusion pressure. However, reasonable pore shape printability ($\sim 1 \pm 0.05$) was observed when pressures of 20 and 30 kPa were maintained. Only one combination of extrusion pressure (30 kPa) and needle translation speed (18 mm/s) was selected based on outstanding strand and pore printability, and was found to facilitate reasonable angle printability ($\sim 1 \pm 0.05$) in 50 mM $CaCl_2$. Strands extruded in 50 mM $CaCl_2$ at 20 kPa pressure maintaining 6–12 mm/s needle translation speed demonstrated reasonable strand and pore printability (~0.9–1) compared to both 100 or 150 mM $CaCl_2$. SEM images revealed that composite PCSA scaffolds incubated in 10 mM PBS maintained their structural arrangement over 3 weeks of incubation. However, the scaffolds lost 55% and 70% of initial mass and elastic modulus, respectively, during the incubation period. In addition, RPSCs incorporated in composite PCSA strands demonstrated somewhat better viability, morphology, and BDNF release compared to that of single PCSA scaffolds. Moreover, composite PCSA strands facilitated better directional neurite outgrowth of neurons compared to controls or single PCSA strands. Therefore, it can be concluded that in future, composite PCSA scaffolds would be useful to use as an artificial nerve graft in regenerating damaged PNS. Since PCSA scaffold was seen to lose 70% of the initial elastic modulus within the first two weeks of in vitro culture, for long term *in vivo* studies it is recommended that the composite PCSA scaffold could be used as a potential filler material in nerve graft fabricated with a mechanically stable synthetic biopolymer.

Data availability

The raw data required to reproduce these findings are available. It can be provided if requested.

Funding

This work was financially supported by the Natural Sciences and Engineering Research Council of Canada [NSERC RGPIN-2014-05648].

Declaration of conflicting interests

The authors declared that they had no conflicts of interest with respect to their authorship or the publication of this article.

Appendix A. Supplementary data

Supplementary data to this article can be found online at https://doi.org/10.1016/j.bprint.2019.e00045.

References

[1] M.D. Sarker, S. Naghieh, N.K. Sharma, X. Chen, 3D biofabrication of vascular networks for tissue regeneration: a report on recent advances, J. Pharm. Anal. 8 (2018) 277–296.
[2] S. Naghieh, E. Foroozmehr, M. Badrossamay, M. Kharaziha, Combinational processing of 3D printing and electrospinning of hierarchical poly(lactic acid)/gelatin-forsterite scaffolds as a biocomposite: mechanical and biological assessment, Mater. Des. 133 (2017) 128–135.
[3] S. Naghieh, M. Badrossamay, E. Foroozmehr, M. Kharaziha, Combination of PLA micro-fibers and PCL-gelatin nano-fibers for development of bone tissue engineering scaffolds, Int. J. Swarm Intell. Evol. Comput. 06 (2017) 1–4.
[4] S. Naghieh, M.R.R. Karamooz Ravari, M. Badrossamay, E. Foroozmehr, M. Kadkhodaei, Numerical investigation of the mechanical properties of the additive manufactured bone scaffolds fabricated by FDM: the effect of layer penetration and post-heating, J. Mech. Behav. Biomed. Mater. 59 (2016) 241–250.
[5] S. Naghieh, A. Reihany, A. Haghighat, E. Foroozmehr, M. Badrossamay, F. Forooghi, Fused deposition modeling and fabrication of a three-dimensional model in maxillofacial reconstruction, Regen. Reconstr. Restor. 1 (2016) 139–144.
[6] J. Terzis, B. Faibisoff, H.B. Williams, The nerve gap: suture under tension vs. graft, Plast. Reconstr. Surg. 56 (1975) 166–170.

[7] M. Sarker, S. Naghieh, A.D. McInnes, D.J. Schreyer, C. Xiongbiao, Regeneration of peripheral nerves by nerve guidance conduits: influence of design, biopolymers, cells, growth factors, and physical stimuli, Prog. Neurobiol. 171 (2018) 125–150.
[8] M.D. Sarker, S. Naghieh, A.D. Mcinnes, D.J. Schreyer, X. Chen, Strategic design and fabrication of nerve guidance conduits for peripheral nerve regeneration, Biotechnol. J. 13 (2018) 1700635.
[9] K.Y. Lee, D.J. Mooney, Alginate: properties and biomedical applications, Prog. Polym. Sci. 37 (2012) 106–126.
[10] S. Naghieh, M. Sarker, M. Izadifar, X. Chen, Dispensing-based bioprinting of mechanically-functional hybrid scaffolds with vessel-like channels for tissue engineering applications – a brief review, J. Mech. Behav. Biomed. Mater. 78 (2018) 298–314.
[11] S. Naghieh, M.R. Karamooz-Ravari, M. Sarker, E. Karki, X. Chen, Influence of crosslinking on the mechanical behavior of 3D printed alginate scaffolds: experimental and numerical approaches, J. Mech. Behav. Biomed. Mater. 80 (2018) 111–118.
[12] S. Naghieh, M. Sarker, M. Karamooz-Ravari, A. McInnes, X. Chen, Modeling of the mechanical behavior of 3d bioplotted scaffolds considering the penetration in interlocked strands, Appl. Sci. 8 (2018) 1422.
[13] J.A. Rowley, D.J. Mooney, Alginate type and RGD density control myoblast phenotype, J. Biomed. Mater. Res. Part A 60 (2002) 217–223.
[14] Y. He, F. Yang, H. Zhao, et al., Research on the printability of hydrogels in 3D bioprinting, Sci. Rep. 6 (2016) 29977.
[15] L. Ouyang, R. Yao, Y. Zhao, et al., Effect of bioink properties on printability and cell viability for 3D bioplotting of embryonic stem cells, Biofabrication 8 (2016) 35020.
[16] F. You, X. Wu, N. Zhu, et al., 3D printing of porous cell-laden hydrogel constructs for potential applications in cartilage tissue engineering, ACS Biomater. Sci. Eng. 2 (2016) 1200–1210.
[17] J.P. Frampton, M.R. Hynd, M.L. Shuler, et al., Fabrication and optimization of alginate hydrogel constructs for use in 3D neural cell culture, Biomed. Mater. 6 (2011), 015002.
[18] A. Khavari, M. Nydén, D.A. Weitz, et al., Composite alginate gels for tunable cellular microenvironment mechanics, Sci. Rep. 6 (2016) 30854.
[19] N.O. Dhoot, C.A. Tobias, I. Fischer, et al., Peptide-modified alginate surfaces as a growth permissive substrate for neurite outgrowth, J. Biomed. Mater. Res. Part A 71 (2004) 191–200.
[20] L. Ning, Y. Xu, X. Chen, et al., Influence of mechanical properties of alginate-based substrates on the performance of Schwann cells in culture, J. Biomater. Sci. Polym. Ed. 27 (2016) 898–915.
[21] M.I. Guenther, N. Weidner, R. Müller, et al., Cell-seeded alginate hydrogel scaffolds promote directed linear axonal regeneration in the injured rat spinal cord, Acta Biomater. 27 (2015) 140–150.
[22] S. England, A. Rajaram, D.J. Schreyer, et al., Bioprinted fibrin-factor XIII-hyaluronate hydrogel scaffolds with encapsulated Schwann cells and their in vitro characterization for use in nerve regeneration, Bioprinting 5 (2017) 1–9.
[23] J.A. Rowley, G. Madlambayan, D.J. Mooney, Alginate hydrogels as synthetic extracellular matrix materials, Biomaterials 20 (1999) 45–53.
[24] J.W. Lee, K.Y. Lee, Dual peptide-presenting hydrogels for controlling the phenotype of PC12 cells, Colloids Surfaces B Biointerfaces 152 (2017) 36–41.
[25] R. Kaewkhaw, A.M. Scutt, J.W. Haycock, Integrated culture and purification of rat Schwann cells from freshly isolated adult tissue, Nat. Protoc. 7 (2012) 1996–2004.
[26] M. Sarker, X.B. Chen, Modeling the flow behavior and flow rate of Medium viscosity alginate for scaffold fabrication with a three-dimensional bioplotter, J. Manuf. Sci. Eng. 139 (2017) 081002.
[27] M. Sarker, M. Izadifar, D. Schreyer, et al., Influence of ionic crosslinkers (Ca2+/Ba2+/Zn2+) on the mechanical and biological properties of 3D Bioplotted Hydrogel Scaffolds, J. Biomater. Sci. Polym. Ed. (2018) 1–29.
[28] M. Sarker, X.B. Chen, D.J. Schreyer, Experimental approaches to vascularisation within tissue engineering constructs, J. Biomater. Sci. Polym. Ed. 26 (2015) 683–734.
[29] L. Ning, H. Sun, T. Lelong, et al., 3D bioprinting of scaffolds with living Schwann cells for potential nerve tissue engineering applications, Biofabrication 10 (2018) 035014.
[30] J. Malda, J. Visser, F.P. Melchels, et al., 25th anniversary article: engineering hydrogels for biofabrication, Adv. Mater. 25 (2013) 5011–5028.
[31] R. Suntornnond, E.Y.S. Tan, J. An, et al., A mathematical model on the resolution of extrusion bioprinting for the development of new bioinks, Materials (Basel) 9 (2016) 756.
[32] V. Brunetti, G. Maiorano, L. Rizzello, et al., Neurons sense nanoscale roughness with nanometer sensitivity, Proc. Natl. Acad. Sci. 107 (2010) 6264–6269.